

# Supplementary Information for Review entitled 'Field-Effect Sensors – From pH sensing to Biosensing: Sensitivity Enhancement using Streptavidin-Biotin as a Model System'

*Benjamin M. Lowe, Kai Sun, Ioannis Zeimpekis, Chris-Kriton Skylaris, Nicolas G. Green*

1. Contents	
1 Reference Electrode Validation Studies	2
2 Threshold Voltage and Surface Potential	3
2.1 MOSFETs	3
2.2 FET-sensors	4
3 MOSFET Drift-Diffusion Equations	5
4 Streptavidin Biochemical Characterisation	6
4.1 Molecular Weight and Sequence	6
4.2 Isoelectric Point	7
4.3 Other Forms	7
4.4 Calculated Charge of Streptavidin	8
5 Summary Table of Streptavidin-sensing Literature	10
6 Frequency-mode Detection	15
7 Methodology for Quantitative Analysis	16
7.1 Literature Discovery Method	16
7.2 Inclusion Criteria	16
7.3 Calculation of 'Sensitivity' Metric	16
7.4 Sensitivity Variation	18
7.5 Paper Specific Notes	19
7.6 Graphs Plotting Details	22
7.6.1 Marker Outline	22
7.6.2 Replots of figures with different scale axis	22
8 Current-Threshold Voltage Relationships	25
9 Linear Region Data	27
10 Biomolecule Binding Reactions and Kinetics	28
10.1 Reaction-Limited Systems	28
10.2 Mass Transport-limited Systems	29
10.3 Concentration-Dependent Response	29
11 Summary of Nomenclature	30
12 References	31

# 1 Reference Electrode Validation Studies

---

It is often stated that a reference electrode (with corresponding liquid-gate potential,  $V_g$ ) is required for a reproducible and stable signal from FET-sensors<sup>1-4</sup>. A conventional reference electrode is not generally suitable for miniaturised biosensors<sup>4</sup> and therefore a pseudo-reference electrode is often used. In this section, various validation studies are reviewed in which the effectiveness of various pseudo-reference electrodes are compared and contrasted.

Chen et al. compared Pt electrodes to a conventional Ag/AgCl electrode (Harvard apparatus inc.), and showed that Pt electrodes are susceptible to current drift and  $\Delta V_T$  shifts due to changes in the redox potential of the electrolyte or addition of external potentials<sup>5,6</sup>.

Rajan (2013) performed detailed experiments which investigate the choice of reference electrode for sensing measurements<sup>7</sup>. Pt pseudo-reference electrode demonstrated larger instability in the current, larger transient signals and increased noise when compared to Ag/AgCl pseudo-reference electrode. Noise-spectroscopy was used to compare Pt and Ag/AgCl pseudo-reference electrodes against a conventional reference electrode (Harvard Apparatus Inc.) and it was found that under static (no-flow) conditions, the low-frequency (approximately 1 Hz) noise levels of all three were similar, however the Ag/AgCl electrodes demonstrated a slightly higher SNR. Under flow-conditions, they observed that the conventional reference electrode performed significantly better, being less susceptible to fluctuations in its surface potential due to the interactions with the fluid-flow. Rajan performed pH sensing experiments in Tris(hydroxymethyl)aminomethane (TRIS) buffer and 4-(2-hydroxyethyl)-1-piperazineethanesulfonic acid (HEPES) buffer and observed pH sensitivities of 25 mV/pH and 12 mV/pH respectively, suggesting the buffer composition had a significant effect on the surface potential of the device or the electrode. The chloride content changed significantly during the TRIS experiment because the HEPES pH was adjusted with NaOH whereas the TRIS pH was adjusted with HCl. Rajan hypothesised the reduction in response was due to changes in the surface potential of the Ag/AgCl pseudo-reference electrode, in which chloride ions are potential determining, and suggest that for optimal results the chloride content should be carefully controlled; for example, by adding KCl/NaCl to the initial buffer solution. To confirm this mechanism, the pseudo-Ag/AgCl reference electrode was compared to the conventional reference electrode and showed negligible response on addition of 1 M NaOH but strong response to the addition 3 M KCl.<sup>7</sup>

To compare the performance of a pseudo-reference electrode to a conventional reference electrode, the open-circuit potential,  $V_{oc,ref}$ , of the two in series can be measured. Rajan (2013) showed that addition of a charged poly-L-lysine resulted in an 80 mV shift  $V_{oc,red}$  for their Pt pseudo-reference electrode, which suggested "bio-fouling", in which biomolecules interfere with the interfacial potential. This further demonstrates that Pt electrodes are unsuitable for usage in FET-biosensing<sup>7</sup>. This result contrasts with that of Ishikawa et al. which showed a stable  $V_{oc,ref}$  on addition of 200 nM streptavidin to 1X PBS<sup>8</sup>.

Upon addition of Bovine Serum Albumin, Minot et al.<sup>3</sup> observed a strong difference in  $V_{oc,ref}$  for their Pt pseudo-reference electrode and therefore recommended usage of a conventional Ag/AgCl electrode. They proposed that the presence of the porous glass frit on the Ag/AgCl electrode separates the metal-solution interface from the analyte solution, thus preventing direct biomolecule adsorption and interference with the interfacial redox reactions and thereby the reference potential.

In contrast to Pt electrodes, Rajan (2013) provided evidence that Ag/AgCl pseudo-reference electrodes are in fact suitable for biosensing experiments (despite the lack of a porous glass frit). In their experiment, upon addition of poly-L-lysine, only 0.1 mV  $V_{oc}$  was observed for the Ag/AgCl pseudo electrode. The pH and biosensing results of Rim et al. support this conclusion, in which on-chip Ag/AgCl pseudo-reference electrode showed a  $V_{oc}$  of < 6 mV and < 1.5 mV for pH and biosensing results respectively<sup>9</sup>.

## 2 Threshold Voltage and Surface Potential

### 2.1 MOSFETs

In order to discuss the threshold voltage, first some MOSFET theory is outlined<sup>10</sup>. In a MOSFET, assuming negligible fixed charges in the oxide, the applied potential ( $\psi_{\text{applied}}$ ) across system is equal to the following:

**Equation 1:** 
$$\psi_{\text{applied}} = \psi_{\text{ox}} + \psi_s + \Phi_{\text{MS}},$$

where  $\Phi_{\text{MS}}$  is the work function difference between the metal and the semiconductor,  $\psi_{\text{ox}}$  is the potential drop across the oxide and  $\psi_s$  is the surface potential at the semiconductor-oxide interface. In MOSFET theory, the surface potential  $\psi_s$  is defined as the amount of band bending in the semiconductor<sup>11</sup>, i.e. the potential difference between the silicon at the surface and the silicon bulk. A potential diagram illustrates this for a simple Metal-Oxide-Semiconductor (MOS) capacitor.

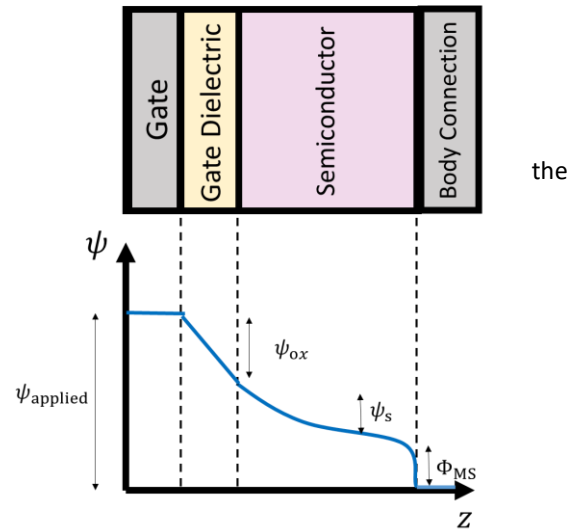


Figure 1 MOS Capacitor potential diagram, adapted from Shinwari et al.<sup>10</sup>

In reality, immobile charges/ions in the semiconductor surface or dielectric, or defects at the interface will modify this potential,  $V$ . These modifications are often modelled as equivalent charges in the insulator-semiconductor surface, i.e. contributing to  $V_{\text{ox}}$  and also to  $\psi_s$  due to the requirement of charge-neutrality.<sup>10</sup>

The surface is inverted when the surface potential  $\psi_s$  is higher than the  $\psi_B$  (defined as  $\psi_B = \psi_f - \psi_i$ ). The term “strong inversion” is used to describe the situation in which the number of charges in the inversion layer,  $n_s$ , are actually significant relative to the semiconductor bulk impurity concentration  $N_A$ . A popular criterion for the point at which “strong inversion” occurs is when  $n_s = N_a$ , since  $N_a = n_i e^{q\psi_B/k_bT}$ , where  $n_i$  is the intrinsic carrier density, and  $N_A$  is the acceptor density (for a p-type device). Therefore the inversion potential can be expressed as:

**Equation 2** 
$$\psi_s(\text{inverted}) \cong 2\psi_B = \frac{2k_bT}{q} \ln\left(\frac{N_a}{n_i}\right)$$

The threshold voltage is defined as the gate voltage that causes the surface potential  $\psi_s$  to reach inversion,  $\psi_s(\text{inv})$ .

**Equation 3:** 
$$V_T = \psi_{\text{ox}} + \psi_s(\text{inverted}) + \Phi_{\text{MS}}$$

Therefore from Equation 1, at strong inversion the threshold voltage is described by the following equation:

$$V_T \cong \psi_{\text{ox}} + 2\psi_B + \Phi_{\text{MS}}$$

Where  $\psi_B = |\psi_f - \psi_i|$  i.e. the potential difference between the fermi potential ( $\psi_f$ ) and the intrinsic fermi potential of the bulk semiconductor ( $\psi_i$ ).

## 2.2 FET-sensors

With FET-sensors, the metal gate present in MOSFETs is replaced by an electrolyte solution containing analyte. A reference electrode is used to provide a reference potential and also sometimes to apply a potential across the device.

A potential diagram for electrolyte-insulator-semiconductor systems has been presented by Bousse (1982)<sup>12</sup> and adapted from Bootsma et al.<sup>13</sup>. Shinwari et al.<sup>10</sup> presented a potential diagram incorporating the reference electrode with potential  $E_{ref}$ . A potential diagram adapted from the review of Shinwari et al. is presented in Figure 2.

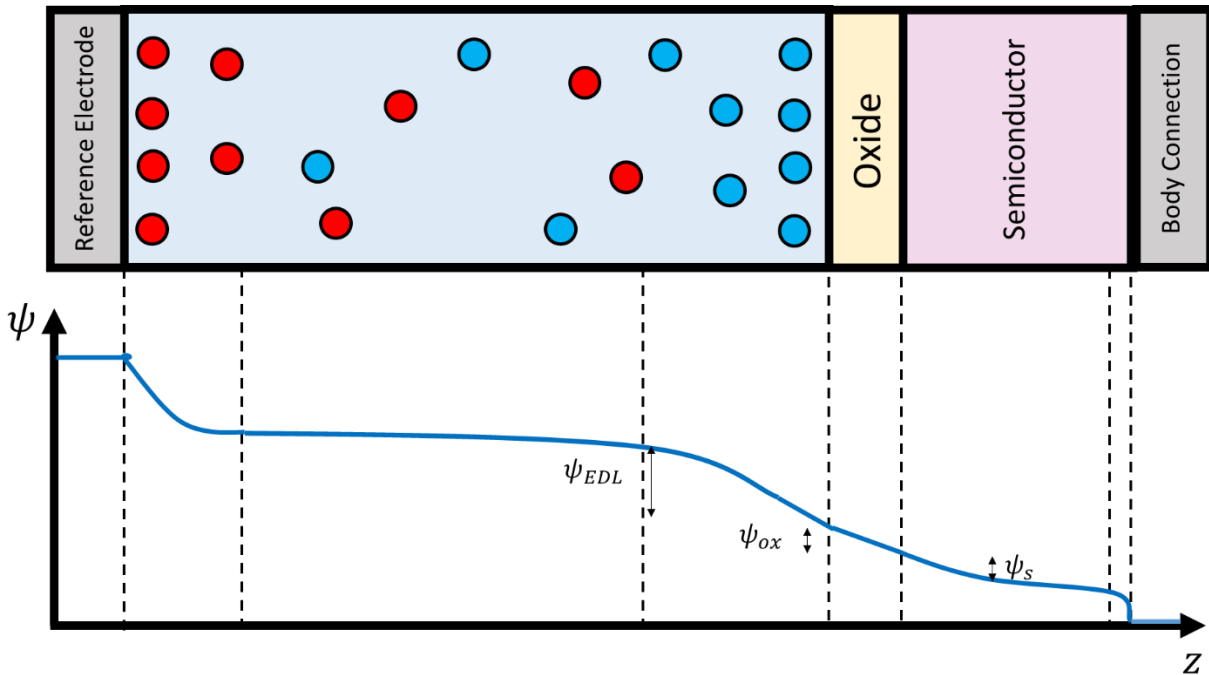


Figure 2 – Electrolyte-insulator-semiconductor potential diagram, e.g. for a FET-sensor. Adapted from Shinwari et al.<sup>10</sup> and Bergveld (2002)<sup>14</sup>

At equilibrium, at the electrode-electrolyte interface, there is an electrostatic potential difference between the bulk electrolyte and the electrode due to polarisation of water and adsorption of ions. Similarly at the oxide-electrolyte interface there is a potential difference due to the electric double layer, which is most commonly modelled using a Gouy-Chapmann-Stern model ( $\psi_{EDL}$ ). This term is often called simply the “surface potential” in electrochemistry, and represents a potential difference from the solid surface to the aqueous bulk, in contrast, the “surface potential” in MOSFET theory often refers to the oxide-semiconductor potential ( $\psi_s$ ), which is the potential change between the semiconductor surface and the bulk of the semiconductor. The oxide layer is usually modelled as a simple capacitor.

Bergveld (whereby in their notation ' $\phi_{ox} - \phi_{sol}$ ' was used, which is equivalent  $\psi_{EDL}$  used in this work) expresses the relationship simply as<sup>15</sup>:

$$V_T = -[c + \psi_{EDL}]$$

Which would imply that on addition of analyte:

$$\Delta V_T = \Delta \psi_{EDL}$$

In agreement with this exact relationship, Jang and Cho<sup>16</sup> equate the magnitude of the change in electrolyte-oxide surface potential with the change in threshold voltage, whilst Rajan et al. and Duan et al implicitly equate them<sup>17,18</sup>.

### 3 MOSFET Drift-Diffusion Equations

Taur and Ning provided a derivation of the relevant drain current equations for a source (n+) – substrate (p) – drain (n+) MOSFET<sup>11</sup>. This derivation utilises the Gradual Channel Approximation which assumes that the electric field in the direction along the channel is much less than the variation in the direction perpendicular to the channel. A further approximation, the Charged Sheet Model<sup>19</sup>, is often made in order to arrive at a closed form expression for the relationship between surface potential and inversion charge. The Charged Sheet Model is based on the observation that the inversion layer is located near the surface of the semiconductor in a thin sheet-like layer<sup>19</sup>. The linear and subthreshold regional approximations of the model are of particular relevance to this work and are presented below:

#### Linear Region

In the linear region, assuming  $V_{ds}$  is small ( $V_g > mV_{ds} + V_T$ , where  $m$  is the body-effect factor), one can obtain the following from the charge-sheet model from the drain current:

Equation 4: 
$$I = \mu_{\text{eff}} C_{\text{ox}} \frac{W}{L} (V_g - V_T) V_{ds}$$

Where  $V_T$  is the threshold voltage, where  $C_{\text{ox}}$  is the oxide capacitance per unit area,  $\mu_{\text{eff}}$  is an effective carrier mobility at some average gate and drain fields,  $W$  is the width of the device and  $L$  is the length of the device.

#### Subthreshold Region

When the gate voltage is low ( $V_g < V_T$ ) the drain current is referred to as the ‘subthreshold current’. In this region, current is dominated by diffusion rather than drift. The following expression can be derived:

Equation 5: 
$$I = \mu_{\text{eff}} \frac{W}{L} \sqrt{\frac{\epsilon_{\text{si}} q N_a}{4 \psi_B}} \left( \frac{k_b T}{q} \right)^2 e^{\frac{q(V_g - V_T)}{m k_b T}} \left( 1 - e^{-\frac{q V_{ds}}{k_b T}} \right)$$

Where  $q$  is the elementary charge,  $\epsilon_{\text{si}}$  is the permittivity of the semiconductor,  $N_a$  is the acceptor impurity density,  $k_b$  is the boltzmann constant and where  $\psi_B = |\psi_f - \psi_i|$  i.e. the potential difference between the fermi potential ( $\psi_f$ ) and the intrinsic fermi potential of the bulk semiconductor ( $\psi_i$ ).<sup>11</sup>. This expression can be reformulated as:

Equation 6: 
$$I = \mu_{\text{eff}} C_{\text{ox}} \frac{W}{L} (m - 1) \left( \frac{k_b T}{q} \right)^2 e^{\frac{q(V_g - V_T)}{m k_b T}} \left( 1 - e^{-\frac{q V_{ds}}{k_b T}} \right)$$

The body-effect factor,  $m$ , is related to the subthreshold slope by:

Equation 7: 
$$SS = \left( \frac{d(\log_{10} I)}{dV_g} \right)^{-1} \approx \frac{\ln(10) m k_b T}{q} \approx \frac{2.3 k_b T}{q} \left( 1 + \frac{C_{\text{dl}}}{C_{\text{ox}}} \right), \quad m = \frac{q \cdot SS}{\ln(10) k_b T}$$

Combining Equation 6 and Equation 7 the following expression is obtained:

Equation 8: 
$$I = \mu_{\text{eff}} C_{\text{ox}} \frac{W}{L} \left( \frac{q \cdot SS}{\ln(10) k_b T} - 1 \right) \left( \frac{k_b T}{q} \right)^2 e^{\frac{\ln(10)(V_g - V_T)}{SS}} \left( 1 - e^{-\frac{q V_{ds}}{k_b T}} \right)$$

Or:

Equation 9: 
$$I_d \propto e^{\frac{q(V_g - V_T)}{m k_b T}}$$

## 4 Streptavidin Biochemical Characterisation

---

In this section, the biochemical data relating to the molecular weight, sequence and isoelectric point are presented in order to understand the charging properties of streptavidin, and hence its expected influence on FET-sensors. Finally, an X-ray crystal structure of streptavidin is used to calculate the net charge of streptavidin using a semi-empirical model.

### 4.1 Molecular Weight and Sequence

In 1986 Argarana et al. sequenced the streptavidin gene, which is shown in the main text, Figure 4. They identified that the first 24 residues (~2.3 kDa) per subunit are likely signal peptide that are removed *in vivo* in the mature protein. The mature protein after *in vivo* processing therefore has 159 residues per sub-unit resulting in a calculated molecular weight of 66 kDa for the protein, which is in close agreement to that measured via sodium dodecyl sulfate polyacrylamide gel electrophoresis (SDS-PAGE) of 70 kDa<sup>20</sup>. They noted a higher molecular weight than that measured in previous work<sup>21</sup> noting that different commercial preparations of streptavidin may have different molecules weight due to the N and/or C-terminal regions being susceptible to proteolytic degradation<sup>20</sup>. More recent work by Wu et al. in 2002 showed a SDS-PAGE molecular weight of 20 kDa per subunit, which was higher than that expected from the sequence, but measurement using Matrix-Assisted Laser Desorption/Ionization (MALDI) mass spectrometry revealed a 16.489 kDa molecular weight per subunit<sup>22</sup>, i.e. 64.9 kDa for the whole protein, in good agreement with the value calculated from the sequence. Others report the weight of streptavidin as approximately 60 kDa<sup>23,24</sup>.

In 1987, Pähler et al. truncated a commercial sample the streptavidin to a minimal size that still retained activity, the advantage of the smaller unit being increased solubility. Their core streptavidin was composed of four heterogenous subunits with a 13.2 kDa average weight, resulting in 52.8 kDa total molecular weight<sup>25</sup>. Thermo Fisher Pierce sells a recombinant form of streptavidin with a reduced molecular weight of 53 kDa<sup>26</sup> which may well be the same structure based on the molecular weight, however the structure is confidential. In 1990, Green provided a review of streptavidin/Avidin properties, which states that “most commercial preparations” were the result of processing of both the N and C termini to give “core” streptavidin of 125-127 residues. They also state “some preparations contain unprocessed streptavidin...”<sup>21</sup>.

The molecular weight of streptavidin is of particular importance as it indicates the similarity between different commercial preparations of streptavidin used in biosensing experiments and therefore the consistency between streptavidin samples. Given the evidence described, different commercial preparations of streptavidin may vary by ~9.2 kDa due to removal of the signalling peptide on the N-terminus *in vivo* and by a further 7.6 kDa via removal of the C terminus by proteolysis. The signalling region contains lysine and arginine (both positively charged residues) per subunit, and the C terminus contains aspartic acid (negatively charged residue) and two lysines per subunit. As streptavidin is a secreted protein, it is likely that all commercial samples will have the signalling peptide removed *in vivo*<sup>20</sup>, however the amount of proteolysis remains unclear between commercial samples and as such it is reasonable to assert that without knowing whether the extent to which streptavidin has been truncated, there may be variability of several net charges per molecule.

## 4.2 Isoelectric Point

### **Bulk Solution Isoelectric Point**

The isoelectric point (pI) quantifies the pH at which a protein is neutral, and is therefore a measure of the charge of a protein in water. Streptavidin is known to have a near-neutral pI; however, likely due to differences in the structure of the biomolecule and difficulty in accurate pI measurement, various values have been reported. Streptavidin from Roche Applied Science is reported to have an estimated pI of between 6.8 and 7.2.<sup>27</sup> Green reported that truncated Streptavidin has a pI of 5-6<sup>21,24,28</sup>. The pI of streptavidin is reported by Sivasankar et al. as approximately 6.3<sup>29</sup>. Rockland™ inc., which sells commercial samples of streptavidin, reports a pI 5-6<sup>30</sup>. Thermo Scientific Pierce sell a recombinant form of streptavidin with a pI of 6.8-7.5 and a molecular weight of 53 kDa. These differences highlight the importance of reporting the source of streptavidin samples for both reproducibility and interpretability of BioFET results.

### **Surface Bound Isoelectric Point**

Surface-bound streptavidin may have different properties to the free protein. The pI of surface-bound streptavidin has been measured by the Surface Force Apparatus (SFA) experiments of Sivasankar et al.<sup>29</sup>. They prepared an orientated monolayer of streptavidin embedded on supported biotin-lipid monolayers and performed SFA measurement of the exposed surface of the streptavidin. The linearized Poisson-Boltzmann equation was used to fit their results, resulting in a calculated pI of 5.0–5.5. This value may be an underestimate due to the neglecting the contribution from the underlying layer which might result in a more positive protein, and therefore a higher pI. There is also error introduced in this calculation based on spatial-averaging and the usage of the linearised Poisson-Boltzmann equations. A more recent study by Almonte et al. using Atomic Force Microscopy (AFM) provided good agreement, in which they calculated a pI of 5.0 +/- 0.5<sup>31</sup>. These studies might suggest that surface-bound streptavidin is slightly more negatively charged than when in bulk solution.

## 4.3 Other Forms

Other forms of streptavidin exist, such as the artificially engineered NeutrAvidin<sup>32</sup> which is a deglycosylated version of avidin with a molecular weight of 60 kDa and a pI of 6.3<sup>26,32</sup>. Monomeric streptavidin has been engineered with reduced affinity for biotin<sup>33</sup>. Genetic modification has been used to deactivate other pockets of streptavidin resulting only a single biotin site<sup>34</sup>.

## 4.4 Calculated Charge of Streptavidin

### Introduction

The net charge of streptavidin has been modelled by De Vico et al.<sup>35</sup> (using PDB ID: 1STP) but their study did not present the charge as a function of pH; at pH 7.4 they calculated a charge of  $-8.49e$  per tetramer. Windbacher et al.<sup>36</sup> state the charge of streptavidin is  $-5e$  but do not provide their methodology. Neither studies consider how structural variation in streptavidin affects the net charge. Lloret et al. used PROPKA (and PDB ID: 1STP) to model the charge of streptavidin as a function of pH predicting a charge of  $-4e$  and  $-5e$  for the 'folded' and 'unfolded' protein, but do not state what structure they used or how it was prepared<sup>37</sup>. Hideshima et al. calculated a charge (based on PDB ID: 1SWE) of approximately  $-1e$ ,  $-2e$  and  $-3e$  at 1X, 0.1X and 0.01X PBS respectively, however their methodology is not reported in sufficient detail for replication<sup>38</sup> within the paper. Based on their other work<sup>39</sup> it was likely performed using a fixed orientation of streptavidin and simply calculating the number of charges per molecule within a 1 Debye length of a plane and each charge was calculated using the Henderson–Hasselbalch equation and literature  $pK_a$  values.

This study aims to provide a more detailed analysis of streptavidin charge as a function of pH and structure.

### Methods

The MOE 2013.08 Software<sup>40</sup> was utilised to perform calculations using the frequently used PROPKA algorithm<sup>41,42</sup>. Charges on the individual amino acids were set using the Henderson-Hasselbalch equation<sup>43</sup> based on their calculated  $pK_a$  values.

All structures were prepared as follows: All explicit water molecules were deleted and the MOE protein preparation tool was used to cap any unterminated groups not resolved in the X-ray structure. The 'Amber10:EHT' forcefield was used, with reaction-field implicit solvation. The 'Protonate3D' algorithm from the MOE software was run using pH 7.4 and 0.1 M ionic strength and the protein was geometry optimised with a harmonic potential restraint of 0.5 Å deviation, so as to remove energetically unfavourable contacts between atoms originating from error in the X-ray structure atomic coordinates. Finally the 'protein properties calculator' was used, which implements the PROPKA algorithm to rapidly calculate the total charge as a function of pH.

The X-ray structure for streptavidin complexed with biotin was obtained from the RCSB Protein Data Bank (PDB ID: 1STP) originally obtained by Weber et al.<sup>44</sup>. This structure is a truncated form of streptavidin. The coordinates of this X-ray structure contain the monomeric form of streptavidin which is constructed into the tetramer using appropriate symmetry within the crystal.

The structure contains a biotin ligand, which has a carboxyl group. However, in a typical biosensing experiment, this carboxyl group would usually not be present. This is because the biotin is covalently immobilised to a surface via its carboxyl group and a long hydrocarbon linker. Hence, in this model the carboxyl group of the biotin was replaced with a methyl group, making it a neutral molecule as would be the situation in a biosensor. Water was removed in all systems and, in order to generate the structure without its ligand, the biotin ligand was removed and the protein minimised using the previously described procedure.

### Results and Discussion

The simulated net charge for the streptavidin protein, as a function of pH, is shown in Figure 3. The stable tetrameric protein, in complex with biotin, showed a simulated pI of 5.04. As expected, on removal of the neutral biotin molecule, the net charge of the protein was insignificantly affected, showing a similar calculated pI of 5.01. This pI is in good agreement with experiments which show pI values in the range 5-6, suggesting the model is performing accurately. Strong chaotropic agents have been reported to result in streptavidin dissociation into its dimeric form<sup>45</sup>, therefore for comparison, the highly solvated monomeric streptavidin structure was also studied. The pI of the monomer was calculated to be 5.66 (with and without the ligand bound), showing a slightly more negative net charge at physiological pH.

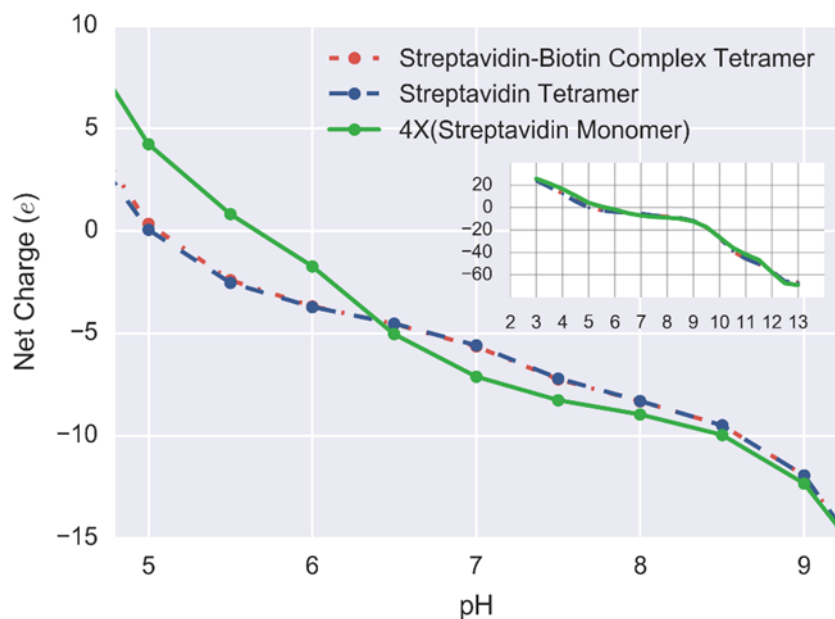


Figure 3 Simulated variation in the net charge of streptavidin versus pH. Three systems were considered: The protein as tetramer in a complex with biotin (red, dashed), with the ligand removed (blue, dash-dot), and, finally, the monomeric form without ligand which is multiplied by four for comparison (green, solid). The inset shows the net charge as a function of pH over the full pH range (2-13). The change in charge due to binding of biotin can be seen by comparing the blue and red curves, and was negligible as expected for a small neutral ligand. Streptavidin is stable in its native tetrameric form however the monomer is shown as an example of the case of dissociation extreme conditions. The monomer has a slightly different titration curve due to its increased solvation.

At pH 7.4, the tetramer was negatively charged with a net charge of approximately  $-7.20e$ , which is the middle of the predictions of the De Vico et al., of  $-8.49e$ <sup>35</sup>, Windbacher et al. of  $-5e$ <sup>36</sup> and Lloret et al. of  $-4e$  to  $-5e$ <sup>37</sup>.

### Conclusion

Depending on the commercial origin of streptavidin, its structure, and hence charge can vary, a fact which has been little appreciated within the BioFET literature. Given the ability of BioFET devices to, in principle, detect elementary charges, this has significant consequences for the comparability and reproducibility of biosensing experiments in which different streptavidin samples are used.

The pH-dependent charge of streptavidin was presented based on a truncated X-ray structure of streptavidin. The predicted pI was 5.04 which is in good agreement with experimental measurements which find a pI of between 5 and 6. The net charge at approximately pH 7.4 is relevant to biosensing conditions, and showed a net charge of  $-7.20e$ , for a truncated structure of streptavidin. A limitation of the semi-empirical methodology used in this work is that it does not account for variation induced by the ionic strength of the solution. The calculated net charge was in between the predictions available within the literature of  $-4e$  and  $-8.49e$ .

## 5 Summary Table of Streptavidin-sensing Literature

---

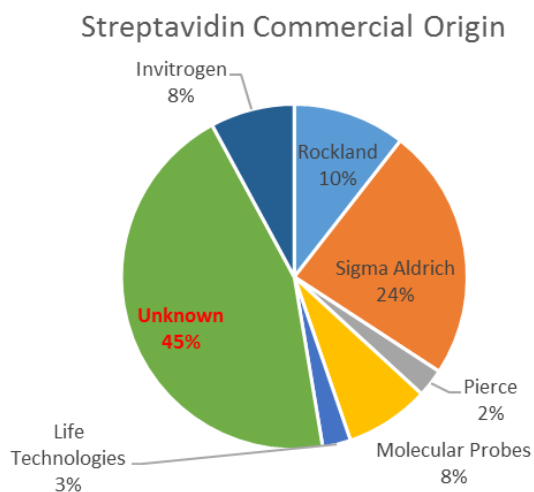
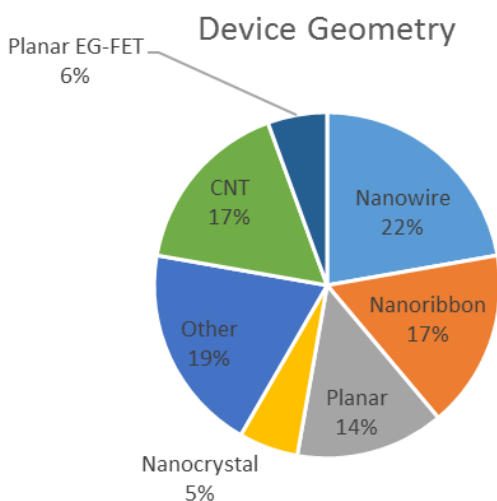
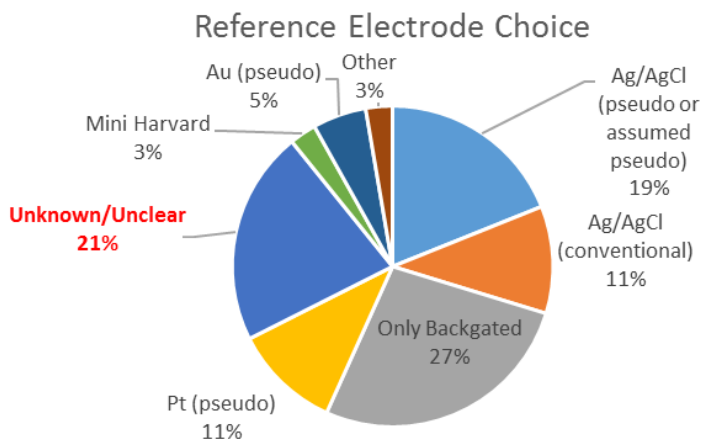
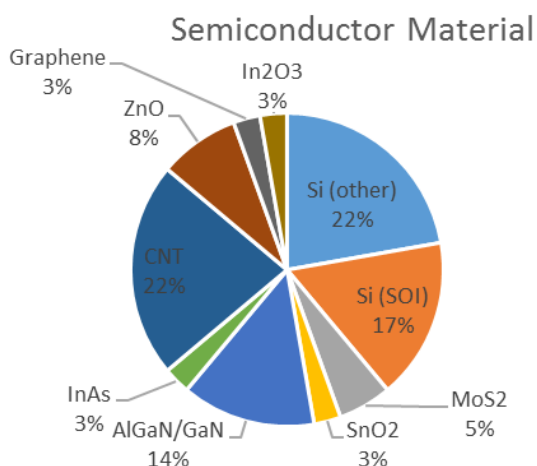
The following table (Table 1) contains a summary of Streptavidin BioFET literature with quantitative response data available. The device behaviour refers to the  $I_{ds}V_g$  response in the region used for sensing, i.e. n-channel means decrease in current with decrease (negative change) in gate voltage. For the Streptavidin Concentration (SAV), the data is sometimes presented as (initial, final, n) where n represents the number of intermediate concentrations separated by 10-fold increases. "No liquid electrode" is used to refer to devices with no electrode in the liquid. SOI = Silicon on Insulator,  $NaP_i$  = Phosphate Buffer. PBS = Phosphate Buffered Saline. EG-FET = Extended-Gate FET, CNT=Carbon Nanotube \*shows characteristics of a Schottky barrier, metal oxide semiconductor field-effect transistor. \*\* On the EG \*\*\* Reported as 30 mM sodium phosphate buffer as 1 X, whereas by convention this would be 3 X. \*\*\*\* Not reported in paper, but in thesis<sup>46</sup>. † Read out via backgate inferred from statement that top gate was fixed for sensing measurements, and sensing measurement shows sweep of ' $V_g$ '. # Assuming 53 kDa molecular weight of streptavidin

<b>Author</b>	<b>Semiconductor Material (Device Behaviour)</b>	<b>Semiconductor-surface Functionalisation</b>	<b>Device Geometry</b>	<b>Buffer</b> 1X PBS = 162.7 mM <sup>37</sup>	<b>SAv Conc. (nM)</b>	<b>SAv Vendor</b>	<b>Electrode (pseudo or conventional)</b>	<b>Mode of Operation for Biosensing</b>
<i>Cui</i> <sup>47</sup>	Si (p-channel)	APTES-biotin	Nanowire	1 mM NaPi (pH 9) with 10 mM NaCl.	250	“Sigma”	No liquid electrode, read via back-gate	?
<i>Stern</i> <sup>48</sup>	SOI (p-channel)	dec-9-enyl-carbamic acid tert-butyl ester (+ biotin?)	Nanoribbon	0.1X PBS	0.01	AlexFluor 655-linked (Molecular Probes) for imaging but ? for the sensing	No liquid electrode, read via back-gate	Subthreshold (Onset of linear for pH sensing)
<i>Shalev</i> <sup>49</sup>	SOI (n-channel)	APTMS-biotin	Nanoribbon	50mM “phosphate buffer” NaPi,?/PBS?	20	?	Ag/AgCl (custom, pseudo)	Subthreshold
<i>Wen</i> <sup>50–52</sup>	AlGaIn/GaN (n-channel)	APTES-biotin	Planar	0.25X PBS	(0.00047, 4.73, 5 10-fold intervals <sup>50</sup> )	?	Pt	Linear and Subthreshold
<i>Sarkar</i> <sup>53</sup>	MoS <sub>2</sub> (n-channel)	HfO <sub>2</sub> -APTES-biotin	Nanocrystals	0.01X PBS	0.00010 and 10000	?	Ag/AgCl (pseudo?)	Linear, Subthreshold and Saturation
<i>Buitrago</i> <sup>54–56</sup>	Si (n-channel)	APTES-biotin	3D Nanowire Array	1X PBS****	0.42	?	Ag/AgCl (conventional commercial, ALS RE-1S)	Subthreshold
<i>Liu</i> <sup>57</sup>	α-Si SOI (n-channel)	SiO <sub>2</sub> -APTMS-biotin	Nanobelt (flow)	0.001X PBS	(0.015, 1.5, 3 10-fold intervals)	Alexa Fluor® 488 Streptavidin (Invitrogen) with 0.1% TWEEN20	Ag/AgCl (pseudo?)	Subthreshold
<i>Cheng</i> <sup>58</sup>	SnO <sub>2</sub> (n-channel)	APTES-biotin	Nanobelt (flow)	1X PBS	0.037	Alexa Fluor® 488 conjugate (Invitrogen)	No liquid electrode. Read out via back-gate	Linear
<i>Ishikawa (2009)</i> <sup>59</sup>	intrinsic In <sub>2</sub> O <sub>3</sub> (n-channel)	Phosphonic acid-based surface + biotin	Nanowire	0.0001X, 0.01X and 1X PBS	100	?	Ag/AgCl (conventional <sup>60</sup> )	Linear
<i>Ishikawa (2010)</i> <sup>8</sup>	Single walled -CNT (p-channel)	None (no biotin, SAv absorb non-specifically)	Nanowire	1X PBS pH 7.4	(0.001, 100, 5 10-fold intervals)	?	Pt (but validated vs Ag/AgCl) liquid gate	Subthreshold for low density structure, at higher density non-transistor-like
<i>Elfström</i> <sup>61–63</sup>	Si SOI (n-channel)	APTES-biotin	Nanoribbon	0.1X PBS	(0.001, 1, 4 10-fold intervals) <sup>61</sup>	Pierce	No liquid electrode, constant back-gate voltage	Subthreshold <sup>64</sup>
<i>Lee (2015)</i> <sup>65</sup>	AlGaIn/GaN (n-channel)	**Au/Ni-SAM-SAv (no biotin, amine coupling)	Planar EG-FET	1X PBS	0.996	Sigma Aldrich	Ag/AgCl (conventional, commercial RE-5B BASi)	Linear
<i>Martínez</i> <sup>66</sup>	Single walled -CNT (Ambipolar)	None. SAv adsorb non-specifically (no biotin)	CNT	2X PBS	?	Aldrich S4762	No liquid electrode, read out via back-gate	CNT: non-traditional transistor $I-V_g$

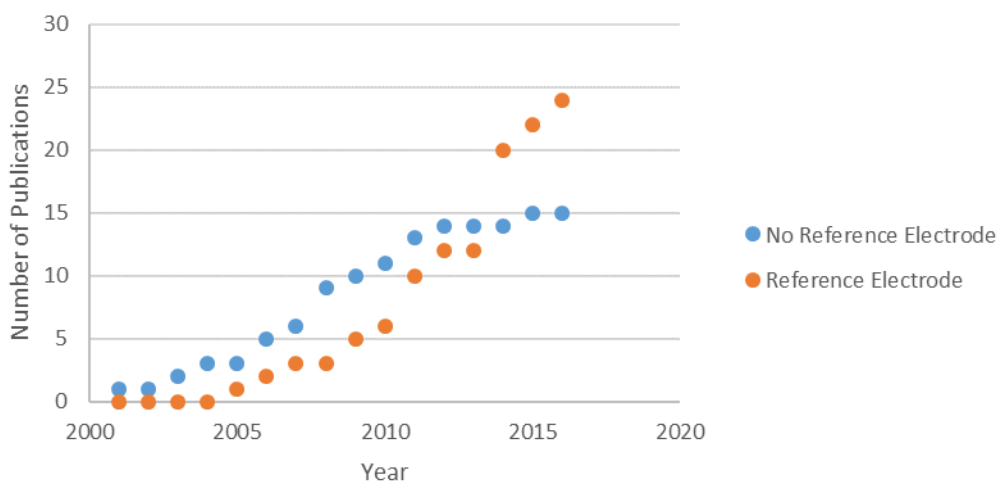
<i>Author</i>	<i>Semiconductor Material (Device Behaviour)</i>	<i>Semiconductor-surface Functionalisation</i>	<i>Device Geometry</i>	<i>Buffer</i> 1X PBS = 162.7 mM <sup>37</sup>	<i>SAv Conc. (nM)</i>	<i>SAv Vendor</i>	<i>Electrode (pseudo or conventional)</i>	<i>Mode of Operation for Biosensing</i>
<i>Duan (2015)</i> <sup>67</sup>	Si SOI (p-channel)	APTES-biotin	Nanowire	~0.01X PBS equiv. (1 mM HEPES)	10	Rockland Immunochemical	? material, commercial Harvard Apparatus "Miniature Reference"	Linear
<i>Duan (2012)</i> <sup>18</sup>	Si SOI (p-channel)	Biotinylated polyelectrolyte (PLL) monolayer	Nanoribbon	~0.01X PBS equiv. (1 mM HEPES)	(0.02, 2, 3 10-fold intervals)	Rockland Immunochemical	Pt top-gate. Read out via back-gate ¶	Full I-V <sub>g</sub> sweep (linear/subthreshold)¶
<i>Upadhyay</i> <sup>68</sup>	Intrinsic InAs (n-channel)	Oxide-BSA-biotin-SAv	Nanowire	0.03X, 0.3X, 3X (***) NaPi	100	?	Ag/AgCl (conventional)	Linear
<i>Gupta</i> <sup>69</sup>	AlGaIn/GaN (n-channel)	APTES-biotin	Planar	Dulbecco's PBS	~16000 #	Alexa Fluor 488 is from Invitrogen Inc. (Carlsbad, CA)	?	?
<i>Star</i> <sup>70</sup>	Single-walled CNT (p-channel behaviour/ambipolar)	PEI/PEG passivation and biotin functionalisation	CNT	~0.1X PBS (0.01 M PBS)	2500	Streptavidin (from Streptomyces avidinii, Sigma Chemicals) with/without Gold label	No liquid electrode, read out via back-gate	CNT: non-traditional transistor I-V <sub>g</sub>
<i>Bradley</i> <sup>71</sup>	Single-walled CNT (p-channel IV behaviour at negative V <sub>g</sub> )	None (non-specific streptavidin binding)	CNT	15 mM NaPi (~1X NaPi)	40	?	"silver" electrode (pseudo?) top-gate. Pt back-gate.	CNT: non-traditional transistor I-V <sub>g</sub>
<i>Kang</i> <sup>72</sup>	AlGaIn/GaN (n-channel)	APTES-biotin	Planar	? mM NaPi	~94,000 #	?	?	?
<i>Choi</i> <sup>73</sup>	ZnO (n-channel)	3-(trimethoxysilyl) propyl aldehyde + biotin-hydrazide	Nanowire	10 mM NaCl (pH 3)	2.5, 25, 250, 1000	FITC labelled Sigma-Aldrich (USA)	? likely no liquid electrode, constant back-gate voltage	<b>Saturation</b>
<i>Ginet</i> <sup>74</sup>	Si (p-channel behaviour)	APTES-biotin	Nanowire	0.01X PBS (pH 5.4)	18.89, 1.88 #	?	Integrated Au top gate	Full IV <sub>g</sub> sweep, non-standard MOSFET characteristic
<i>Hsiao</i> <sup>75</sup>	Poly-si (n-channel behaviour)	APTES-biotin	Nanowire	0.1X PBS (10 mM, pH 7.4)	0.00017, 0.0167, 1.67, 167	Sigma-Aldrich (USA)	no liquid electrode, constant back-gate voltage	Full IV <sub>g</sub> Sweep, data shown in linear region based on dry-device.
<i>Jeon</i> <sup>76</sup>	ZnO (n-channel)	3-(trimethoxysilyl)propyl aldehyde+ biotin	Nanowire	1 mM "phosphate buffer" with 10 mM NaCl (pH 8)	2.5, 25, 250, 1670	FITC-labelled, ? origin	? likely no liquid electrode, constant back-gate voltage	? (no IV data)
<i>Khatayevich</i> <sup>77</sup>	Graphene (?-)	biotin-graphite binding peptide	Graphene	"used as received"	Multiple concs.	Sigma-Aldrich, USA	?	?

<i>Author</i>	<i>Semiconductor Material (Device Behaviour)</i>	<i>Semiconductor-surface Functionalisation</i>	<i>Device Geometry</i>	<i>Buffer</i> 1X PBS = 162.7 mM <sup>37</sup>	<i>SAv Conc. (nM)</i>	<i>SAv Vendor</i>	<i>Electrode (pseudo or conventional)</i>	<i>Mode of Operation for Biosensing</i>
<i>Jim Suk Kim</i> <sup>78</sup>	ZnO (n-channel)	PEG-biotin	"nanorod" (nanowire)	~0.1X PBS ("0.01 M PBS pH 7.2")	25, 250, 2500	?	? likely no liquid electrode, constant back-gate voltage	Unclear due to strong hysteresis, but not subthreshold.
<i>Won Hee Lee</i> <sup>79</sup>	Si (n-channel)	APTES-biotin	Nanoribbon	0.01X, 0.1X, 1X PBS	buffer, 0.001, 0.01, 1	?	? "liquid gate"	Subthreshold (+Full I-V <sub>g</sub> graph)
<i>Nam</i> <sup>80</sup>	MoS <sub>2</sub> (n-channel) and WSe <sub>2</sub> (ambipolar)	APTES-biotin	Nanocrystals	PBS (? pH/ionic strength)	Buffer, [7x10 <sup>-6</sup> , 7x10 <sup>-2</sup> , 4 intervals]	?	no liquid electrode, constant back-gate voltage	Full I-V <sub>g</sub> available with linear y-axis,
<i>Hu (2011)</i> <sup>81</sup>	Single-walled CNT	PEI/PEG-biotin	CNT	0.1X PBS ("10 mM PBS, pH 7.4")		Molecular Probes	no liquid electrode, constant back-gate voltage	CNT: non-traditional transistor I-V <sub>g</sub> .
<i>Wang</i> <sup>82</sup>	AlGaIn/GaN (n-channel)	APTES-biotin	Planar (recessed)	1X PBS	Buffer, 16x10 <sup>-5</sup> ,	?	Pt liquid gate electrode (V <sub>g</sub> =0 for sensing)	Subthreshold
<i>Im</i> <sup>83</sup>	SOI wafer (p-channel)	Nanogap with gold layer-SAM-biotin confined near the surface oxide	Nanogap	Performed on <b>dry device</b>	300	?	Au integrated gate	Full I-V <sub>g</sub> sweep available (log y-axis)
<i>Dong-Sun Kim</i> <sup>84</sup>	Si (n-channel)	Au-SAM-biotin	Planar EG-FET	K <sup>+</sup> PBS <b>pH 6.4</b> , 20 mM K	1886 #	Pierce, Rockford, IL	Ag/AgCl liquid gate electrode	Full I-V <sub>g</sub> sweep available (linear y-axis)
<i>Han</i> <sup>85</sup>	Si (n-channel)	Au-SAM-biotin	Planar (3D structured)	K <sup>+</sup> PBS <b>pH 6.4</b> , 20 mM K	18.86 #	?	Ag/AgCl liquid gate electrode	Full I-V <sub>g</sub> sweep available (linear y-axis)
<i>Jacquot</i> <sup>86</sup>	AMIS CMOS	SAM + biotinylated BSA	"Chemoreceptive neuron" MOS	0.1X pH 7.4	0.377 #	Pierce, Rockford, IL	None - Novel mode of operation (dry-device)	Novel mode of operation (dry-device)
<i>Hu (2008)</i> <sup>87</sup>	Single-walled CNTs	Biotin	CNT	~0.1X "0.02 M, pH 7.2"	50	Molecular Probes	no liquid electrode, constant back-gate voltage	CNT: non-traditional transistor I-V <sub>g</sub>
<i>Münzer</i> <sup>88</sup>	Single-walled CNTs	Biotin-	CNT	Universal buffer (Britton-Robinson) at various pH	140?	Life Technologies	Ag/AgCl liquid gate electrode	CNT: non-traditional transistor I-V <sub>g</sub>
<i>Kulkarni</i> <sup>89,90</sup>	Single-walled CNT	Non-covalently bound biotin-	CNT	0.001,0.01,0.1 M NaCl	?	?	(suspended liquid top-) gate electrode formed by evaporating Cr/Au	Frequency mode detection

The following pie charts summarise some of the categorical properties from the table:



In addition, whether or not Ag/AgCl (pseudo or assumed pseudo), Ag/AgCl (conventional), Pt (pseudo), Mini Harvard and Au (pseudo) electrodes were grouped into one category and compared to the backgate-only case, and plotted as a function of time:



## 6 Frequency-mode Detection

---

Despite a range of theoretical papers on SNR in oxide-electrolyte systems<sup>91–98</sup>, experimental measurement of time-varying noise has so far often been limited to systems without biomolecules<sup>99–105</sup>, with only a few studies to-date which investigate frequency response of the device for biomolecular response<sup>89,90,106–109</sup>.

In 2010, Zheng et al. introduced a novel FET-based bimolecular detection methodology in which the frequency-domain of the current response was used<sup>107</sup>. With buffer upon the FET-sensor surface, they observed the typical  $1/f$  noise for MOSFET devices but on addition of prostate-specific antigen they observed a characteristic Lorentzian response in the kHz region, the frequency of which was related to the surface-receptor (antibody) density, but was independent of analyte concentration, and rationalised their results in terms of thermal noise due induced by the antigen layer. Importantly, the limit of detection (defined qualitatively as the region in which it was not “difficult to distinguish” the signal from the noise) was 30 times improved compared to time-based measurements<sup>107</sup>. Georgakopoulou et al. later provided a mathematical analysis supporting the notion of the noise being induced by thermal noise, and highlighting the possibility of frequency-mode detection for simultaneous detection of various analytes<sup>110</sup>, an idea that has received attention in the wider biosensing community<sup>108</sup>. Chung et al. recently performed a particle-based simulation in which charged spherical particles approach the FET-surface<sup>111</sup>. In their work, the noise levels increased as the particles approached, and the results strongly suggest that the thermal-Coulombic motion of ions gathered around the particles induce the Lorentzian shapes in the noise spectrum. Frequency mode detection is increasingly receiving attention within this field<sup>112,113</sup>.

## 7 Methodology for Quantitative Analysis

### 7.1 Literature Discovery Method

In order to discover publications for this review. Scopus was searched with the following term in December 2016: ( TITLE-ABS-KEY ( biofet OR fet OR field-effect transistor OR field-effect device OR fed OR field effect ) AND TITLE-ABS-KEY ( streptavidin ) OR CHEMNAME ( streptavidin ) )

This was supplemented by a search of Thomson Reuter's Web of Knowledge search engine in early 2016 for keywords BioFET and streptavidin.

### 7.2 Inclusion Criteria

The criteria for inclusion in the quantitative analysis were as follows:

If both time-dependent current data and  $I_{ds}$ - $V_g$  data was available, the time-dependent data was used for current response extraction. If the device showed a non-typical  $I_{ds}$ - $V_g$  graph such that region of operation could not be identified (linear vs subthreshold), or shows effects indicative of a response which is not due to electrostatic gating (e.g. via a significant change in the shape of the  $I_{ds}$ - $V_g$  graph), it was excluded from the quantitative analysis. The subthreshold slope and region of operation is poorly defined in such cases (e.g. <sup>78</sup>).

The requirement of a similar surface chemistry is needed for quantitative comparison of the results, as the device measures changes in surface potential. Papers included in the quantitative analysis (i.e. Figures 7 and 9) structures must incorporate an oxide-(APTES or APTMS)-biotin functionalised sensor-surface which undergoes streptavidin binding.

Streptavidin which was attached to a particle, such as streptavidin-labelled (magnetic) particle, were excluded. Papers were excluded if the experiment was such that streptavidin was bound to the surface and the response was measured as a function of biotin concentration. Papers in saturation mode were excluded (e.g. Choi et al. <sup>73</sup>) but included in the tabular summary of literature. Papers in which a gold-self assembled monolayer-biotin surface were used were excluded but included in the tabular summary of literature.

Carbon-nanotube based device results are not the focus of this work as they can operate via non-electrostatic gating mechanisms. These devices were excluded for quantitative comparison but many are included in the tabular summary in Supplementary Information Table 1.

The nanogap devices of Im et al.<sup>83</sup> exhibited a substantial change in the I- $V_g$  graph ( $I_{norm}^+$  (~200,000%)) after streptavidin binding however their device operates under dry-conditions and therefore a different mechanism of operation, and was not included.

### 7.3 Calculation of 'Sensitivity' Metric

In principle the sensitivity could be obtained using the IUPAC definition of sensitivity, in which the gradient of a concentration response-calibration curve would provide the sensitivity. However, it is not uncommon for the Normalised Change in Current to be used as the response readout, and this metric is a measure of the change in current with analyte concentration. Therefore, in this work the Normalised Change in Current was used as the basis for the metric 'Sensitivity' as was defined as described in the main text and in more detail in this section.

$I_i$  is the current at the  $i$ th 10-fold increase in analyte concentration, so  $I_{i+1}$  is the current at 10-fold higher concentration of analyte than  $I_i$ .

**Equation 10:**

$$I_{norm,i} = \frac{I_{i+1}}{I_i} - 1$$

In this calculation, the value of  $\Delta I$  used in calculating each  $I_{norm,i}$  is taken to be between each subsequent measurement (as opposed to an initial control drain current and each measurement).

For  $n$  10-fold changes in analyte concentration, the highest current ( $i = n$ ) can be calculated from the lowest current ( $i = 0$ ) and the Normalised Change in Current ( $I_{\text{norm}}$ ) using:

**Equation 11:** 
$$I_n = I_0(I_{\text{norm},i} + 1)^n$$

Assuming that values for  $I_i$  are taken such that the response has not saturated, and assuming that  $I_{\text{norm}}$  is constant with 10-fold increase in analyte concentration, then this  $I_{\text{norm}}$  corresponds to the representative Normalised Change in Current per 10-fold increase in analyte concentration, and is referred to as Sensitivity herein; therefore solving for constant  $I_{\text{norm}}$  in the above equation:

**Equation 12:** 
$$\left(\frac{I_n}{I_0}\right)^{\frac{1}{n}} - 1 = I_{\text{norm}} = \text{Sensitivity}$$

For example, from pH 5 to pH 9 with an n-channel device, the unbounded Sensitivity would be calculated as:

**Equation 13:** 
$$\left(\frac{I_{\text{pH5}}}{I_{\text{pH9}}}\right)^{\frac{1}{4}} - 1 = \text{Sensitivity}$$

As a biosensing example, taking the streptavidin-sensing data of Won Hee Lee et al.<sup>79</sup>, the calculation of Sensitivity can be seen in

:

**Table 2** Tabular example of calculation of Sensitivity values from literature data. Current values from Won Hee Lee et al.<sup>79</sup> were used to calculate Sensitivity using Equation 12. The measurement spans three 10-fold increases in streptavidin concentration ( $n = 3$ ).

Concentration (pM)	$I_i$ (A)
1	4.57E-9
1000	7.3E-10
Unbounded Sensitivity (used in this work) (%)	83.84

As sometimes authors only report  $I_{\text{norm}}$  (as opposed to the current), it is also useful to calculate Sensitivity from  $n$  values of  $I_i$ .

**Equation 14:** 
$$I_n = I_0 \prod_{i=0}^n (I_{\text{norm},i} + 1)$$

Inserting

Equation 14 into

Equation 12 we obtain the Sensitivity as a function of a set of available  $I_{\text{norm},i}$  measurements:

$$\left(\frac{I_n}{I_0}\right)^{\frac{1}{n}} - 1 = \left(\frac{I_0 \prod_{i=0}^n (I_{\text{norm},i} + 1)}{I_0}\right)^{\frac{1}{n}} - 1 = \left(\prod_{i=0}^n (I_{\text{norm},i} + 1)\right)^{\frac{1}{n}} - 1 = \text{Sensitivity}$$

This Sensitivity is equivalent to that in

Equation 12. For example from pH 5 to pH 9 with an n-channel device, the unbounded Sensitivity would be calculated as:

**Equation 15:** 
$$I_{\text{norm.pH6}} = \frac{I_{\text{pH6}} - I_{\text{pH5}}}{I_{\text{pH5}}} = \frac{I_{\text{pH6}}}{I_{\text{pH5}}} - 1$$

**Equation 16:** 
$$(I_{\text{norm,pH6}} + 1) \cdot (I_{\text{norm,pH7}} + 1) \cdot (I_{\text{norm,pH8}} + 1) \cdot (I_{\text{norm,pH9}} + 1)^{\frac{1}{4}} - 1 = \text{Sensitivity}$$

As sometimes only  $I_{\text{norm}}^-$  is reported sometimes  $I_{\text{norm}}^-$  was converted into  $I_{\text{norm}}^+$  using the following method. First recall that:

**Equation 17:** 
$$I_{\text{norm}}^- = \left( \frac{I_{\text{low}}}{I_{\text{high}}} - 1 \right) 100$$

Therefore it follows that:

**Equation 18:** 
$$I_{\text{norm}}^+ = (I_{\text{norm}}^- + 1)^{-1} - 1$$

As an biosensing example, taking the streptavidin-sensing data of Wen et al<sup>50</sup>, the calculation of Sensitivity can be seen in Table 3.

**Table 3 – Tabular example of calculation of Sensitivity values from literature data.  $I_{\text{norm}}^-$  (%) values from Wen et al.<sup>50</sup> was converted to  $I_{\text{norm}}^+$  using Equation 18 and then Sensitivity values were calculated using Equation 14.**

Concentration (pM)	$I_{\text{norm}}^-$ (%)	$I_{\text{norm}}^+$ (%)
0.473	-6	6.38298
4.73	-9.97	11.0741
47.3	-37.82	60.8234
473	-43.28	76.3047
4730	-67.26	205.437
Bounded Sensitivity (%)	-37.19	
Unbounded Sensitivity (used in this work) (%)		59.22

Given the effect of ionic strength on device response and variability between streptavidin preparations from different commercial sources, ideally these factors would be constant when comparing experiments. However the varied nature of the research experiments means that this comparison unavailable at the time of writing.

## 7.4 Sensitivity Variation

MOSFET theory predicts that the ability of the semiconductor to transduce a change in surface potential to a change in current ("change per decade"/Sensitivity) should be independent of the magnitude of the threshold voltage change, assuming the response remains within the subthreshold region. However, the change in threshold voltage could theoretically be different between the limit of detection (low analyte concentration) and analyte-saturation (high analyte concentration).

In the following we first discuss this in the context of pH sensing and biosensing data separately:

For pH sensing, the response at in the pH range most relevant to biosensing (pH 6-8) is approximately linear for a range of oxides<sup>114</sup>. Silica in particular is well known to have an unusual shape to its surface charge-pH curve<sup>115</sup> and we present a summary figure below which shows that it is also approximately linear in the 6-8 pH range.

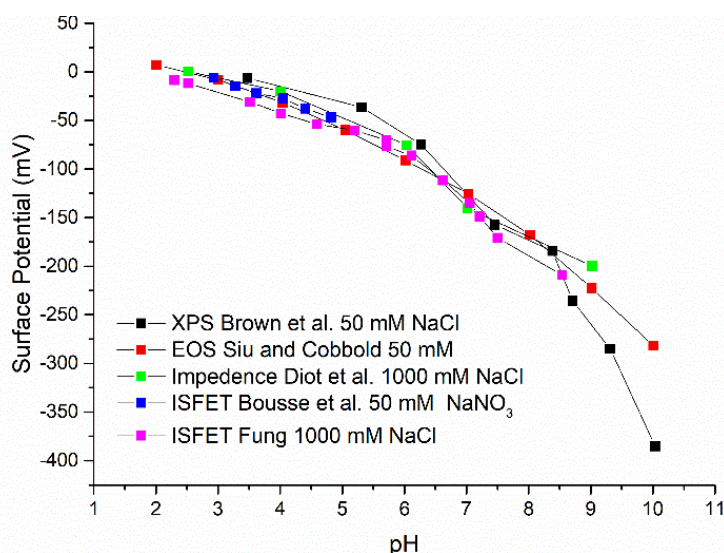


**Figure 4: Surface potential measurements of the silica-water interface extracted from the literature. In the pH range most relevant to biosensing (~pH 6-8), silica typically demonstrates  $33 \pm 3$  mV/pH. The legend shows the measurement technique, first author and electrolyte composition. XPS=X-ray Photoelectron Spectroscopy<sup>116</sup>, EOS (Electrolyte-Oxide-Semiconductor)<sup>117</sup>, Impedance measurement on EOS system<sup>118</sup>, IS-FET (Ion-Sensitive Field-Effect Transistor) of Bousse et al.<sup>119</sup>, Fung et al.<sup>120</sup>.**

For biosensing, at high analyte concentrations, analyte-saturation occurs with a corresponding reduction in binding per 10-fold increase in analyte concentration is expected. With the exception of Elfström et al., we saw no evidence of analyte-saturation in the papers shown in Figure 9 of the main text, which may be because these publications measured across relatively narrow concentration ranges (three to five 10-fold increases in concentration), so do not reach saturation. Alternatively (or in addition to this), it may be because at high concentrations increased non-specific binding occurs, which results in additional non-specific response even beyond saturation of the receptors on the sensor surface. Elfström et al. demonstrated a linear increase in current with 10-fold increase in analyte followed by a negligible change in response due to analyte saturation. (This saturated data point was excluded from the analysis as explained in the supplementary information, paper-specific notes section 7.5)

## 7.5 Paper Specific Notes

This meta-analysis involved extraction of data for many literature sources. Some of the papers reported their data with some ambiguity, and therefore in this appendix paper-specific notes are provided which explain any assumptions made and any notes regarding uncertainty of the literature data.

**Buitrago et al.<sup>55</sup>**

Did not allow the system to fully equilibrate as their system was immediately washed with buffer<sup>46</sup>, so their extracted Sensitivity is underestimated.

**Cui et al.<sup>47</sup>**

Did not state the region of operation. The region was assumed to be in the subthreshold region with a subthreshold slope of 0.962 estimated from their pH sensing data. This calculation was based on their measured pH Sensitivity of ~9% and an assumed value of 33 mV/pH for the oxide dielectric.

**Duan et al.<sup>18</sup>**

Measured response over a range of streptavidin concentrations. As the region of operation and top gate threshold voltage shift cannot unambiguously be extracted from the publication, these results were not included in the quantitative analysis within the main text of the review. In more detail: Although a full  $I-V_{g,back}$  curve is presented for one concentration, it is plotted with a linear-current axis making subthreshold data difficult to extract from this figure directly. They state that the gate voltage “was determined from  $I_d-V_g$  measurement before sensing.” however they do not state the gate voltage used in each biosensing measurements presented, making the region of operation unclear for some measurements. The gate reported is a backgate, and therefore their measured shift of 320 mV in threshold voltage does not correspond to the electrolyte-oxide surface potential but is an amplified signal related to the electrolyte-oxide surface potential.

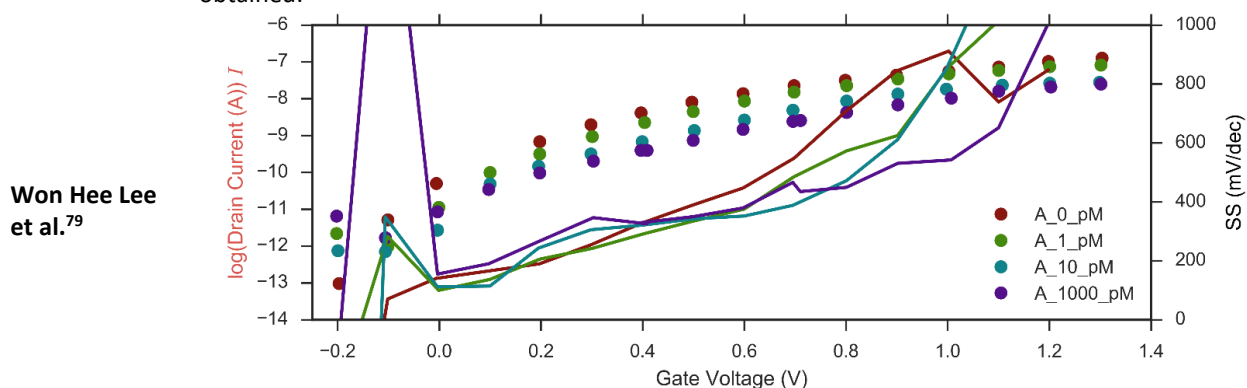
**Elfström<sup>61</sup>**

The measurement recorded at concentration of  $1 \times 10^8$  M streptavidin, was excluded from the analysis in the main text as the sensor response was deemed to have saturated, showing a less than a 1% increase in sensitivity with a 10-fold increase in sensitivity.

The region of operation was not specified for the work of Elfström et al.<sup>61</sup> however personal communication stated it was operated in the subthreshold region<sup>64</sup>. Their device was operated without a reference electrode.

This conference paper reported a high change in current and threshold voltage per 10-fold increase in streptavidin concentration. A key claim of the paper is that the subthreshold slope changes with streptavidin concentration.

Here, a centred-difference numerical derivative of their  $I-V_g$  data from their Figure 2a was used to extract their subthreshold slope as a function of gate voltage, and the following graph was obtained:



The solid lines show the interpolated subthreshold slope, and the dots show their extracted data. It can be seen that the subthreshold slope remains relatively concentration independent at  $\sim 200$ - $400$  mV/dec, in direct contraction to a key claim of the paper. The reliability of this conference paper is put into doubt because the data does not seem to support their conclusions.

Won Hee Lee et al. refer to a liquid gate in their discussion but do not state whether this is an electrode and if so, its material, making it ambiguous how the device was gated.

Liu et al.<sup>57</sup>

Provided both the percentage change in current and measured change in threshold voltage as a function of concentration of streptavidin. The Sensitivity value extracted from their current-response data was 7.48%. Therefore the calculated  $\Delta V_T$  per 10-fold increase in analyte concentration was 3.82 mV/p[A] using their reported subthreshold slope of 0.122. The shift in threshold voltage per 10-fold increase in analyte concentration, obtained by linear regression of the *measured*  $\Delta V_T$  against  $\log([\text{streptavidin}])$ , was 8.52 mV per 10-fold increase in analyte concentration. i.e. an error of 4 mV was introduced in the analysis within this review by using the current response to threshold voltage relationship to plot the result in Figure 9 of the main text of this review.

Sarkar et al.<sup>53</sup>

Measured a streptavidin concentration-dependent response, however as the conditions under which the experiments was performed cannot unambiguously be extracted from the publication, this data was not included in the quantitative analysis presented in the main text. In more detail: within the work of Sarkar et al. it is unclear what precise conditions are used in their Figure 4 subfigures. In their Figure 4a, the results were likely obtained at  $\sim \text{pH } 7.4$  because PBS was used, but the device was operated in the linear region so not included in the work presented in this thesis. They show data in highly acidic conditions in a different subfigure. The data in their Figure 4f was obtained in the subthreshold region, however their work does not specify the pH at which this was operated. As a result, the pH may be significantly different and thereby the charge on streptavidin different to other work performed at  $\sim \text{pH } 7.4$ . Because of these limitations, their data was not included in the quantitative analysis in the main text.

Sarkar et al.<sup>53</sup> defined Sensitivity as “the ratio of the difference in current before and after biomolecule binding to the lower of the two currents” which is the definition of  $I_{\text{norm}}^+$  in this review. They state that all experiments were done with “comparatively thicker” MoS<sub>2</sub> flakes, resulting in a higher Subthreshold Slope value, but for their Figure 4e they used thinner flakers with only four atomic layers in order to obtain improved Subthreshold Slope. They report a subthreshold slope of 90 mV/dec, although it is not entirely unambiguous as to which device this subthreshold slope corresponds.

Their Figure 4a provides a measurement in 0.01X PBS at 10  $\mu\text{M}$  concentration of streptavidin, and based on the high drain currents ( $\mu\text{A}$ ) it is assumed that this is in the linear region for the analysis in this work.

<p><b>Shalev et al.</b><sup>49</sup></p>	<p>The current response was provided in their Figure 11 as a function of drain-source voltage (<math>V_{ds}</math>) and the calculated Sensitivity varied between ~50-170% depending on the choice of <math>V_{ds}</math>. The highest value of 170% (at the lowest drain-source) voltage, was presented in the main text.</p> <p>The buffer was “50 mM phosphate buffer”: it is ambiguous whether this is PBS or sodium phosphate. For this work it was taken as equivalent to ~0.3X PBS (where 1X PBS has an ionic strength of 162.7 mM).</p>
<p><b>Stern et al.</b><sup>48</sup></p>	<p>The data from the publication was not included in the quantitative analysis figures in the main text of this review because the surface functionalisation was not oxide-APTES-biotin, instead they utilised chemistry to selectively functionalise the nanowires involving dec-9-enyl-carbamic acid tert-butyl ester.</p> <p>Two data points were shown for the streptavidin sensing result of Stern et al.<sup>48</sup>, these are not two separate experiments but one experiment. In their work, the biosensing current response was normalised by ‘pre-addition average current’, but it is ambiguous whether this was done after each addition, or normalised to the original addition and therefore two possible (unbounded) Sensitivity values could be calculated 59% and 33%; only one of which is correct. The Subthreshold Slope for the device used for biosensing was not reported.</p>
<p><b>Wang et al.</b><sup>82</sup></p>	<p>The Sensitivity extracted in this work is based on the difference in response measured upon increasing concentration of Streptavidin between 16 fM and 16 aM. As this is based on only one log-unit change in concentration, it is less reliable than the Sensitivity values extracted from other papers which incorporate several log-unit changes. Detection of 16 fM using 0.5 microlitre volume would correspond to only 5 streptavidin molecules and therefore would suggest an extremely good detection limit, however the publication does not provide evidence of reliability (e.g. repeat experiments) and specificity (e.g. biotin cleavage).</p>
<p><b>Wen et al.</b><sup>50</sup></p>	<p>The Subthreshold Slope was obtained from their Figure 2 of 0.19 V/dec, and this value has an error of approximately +/- 0.1 V/dec due to the curvature of their I-V characteristic; they report 3.208 dec/V (0.3117 V/dec).</p> <p>It is unclear whether the <math>I_0</math> used in their sensitivity values is from before any streptavidin was added or after the previous addition of streptavidin, however if it was the former then the linear sensitivity values would increase monotonically therefore it was assumed that it is the latter.</p> <p>It is unclear whether their sensitivities calculated in their work are <math>I_{norm}^+</math> or <math>I_{norm}^-</math>. In their Figure 4 they provided negative values suggesting <math>I_{norm}^-</math> but in their table they give positive values. In this work it was assumed they were all calculated as <math>I_{norm}^-</math> and so their values were converted to <math>I_{norm}^+</math> for comparison in the graphs presented in the main text.</p> <p>Their extracted Sensitivity value was 36.8%. Therefore calculated <math>\Delta V_T</math> per 10-fold increase in analyte concentration was 26 mV/p[A] using a subthreshold slope of 0.19. The shift in threshold voltage per 10-fold increase in analyte concentration, obtained by linear regression of their <i>measured</i> <math>\Delta V_T</math> against <math>\log([\text{streptavidin}])</math>, was only 7.4 mV per 10-fold increase in streptavidin concentration. This shows that an error is introduced in the analysis in this review by using the current response to threshold voltage relationship to plot the result in Figure 9b of the main text of the review.</p>

## 7.6 Graphs Plotting Details

### 7.6.1 Marker Outline

For figures in the quantitative analysis of the main text in which marker outline thickness was related to ionic strength, the thickness was set as follows. If the buffer used was PBS, the dilution was recorded (e.g. 1X = 1, 0.1X = 0.1 etc.). If the buffer was not PBS, the dilution factor for a PBS solution with equivalent ionic strength was used assuming 1X PBS is 162.7 mM. Finally, each data point was assigned one bin based on its dilution value using the following half-open intervals:

(0,0.2500001], (0.2500001, 0.500001], (0.50001, 1.00001], (1.00001, infinity]

resulting in each measurement being assigned a bin from low to high ionic strength with each bin being a linearly thicker marker than the previous bin. The marker width was chosen such that the thickest was the highest ionic strength.

The following includes re-plots of the figures from the main text using linear scales for the different axis rather than log scales.

### 7.6.2 Replots of figures with different scale axis

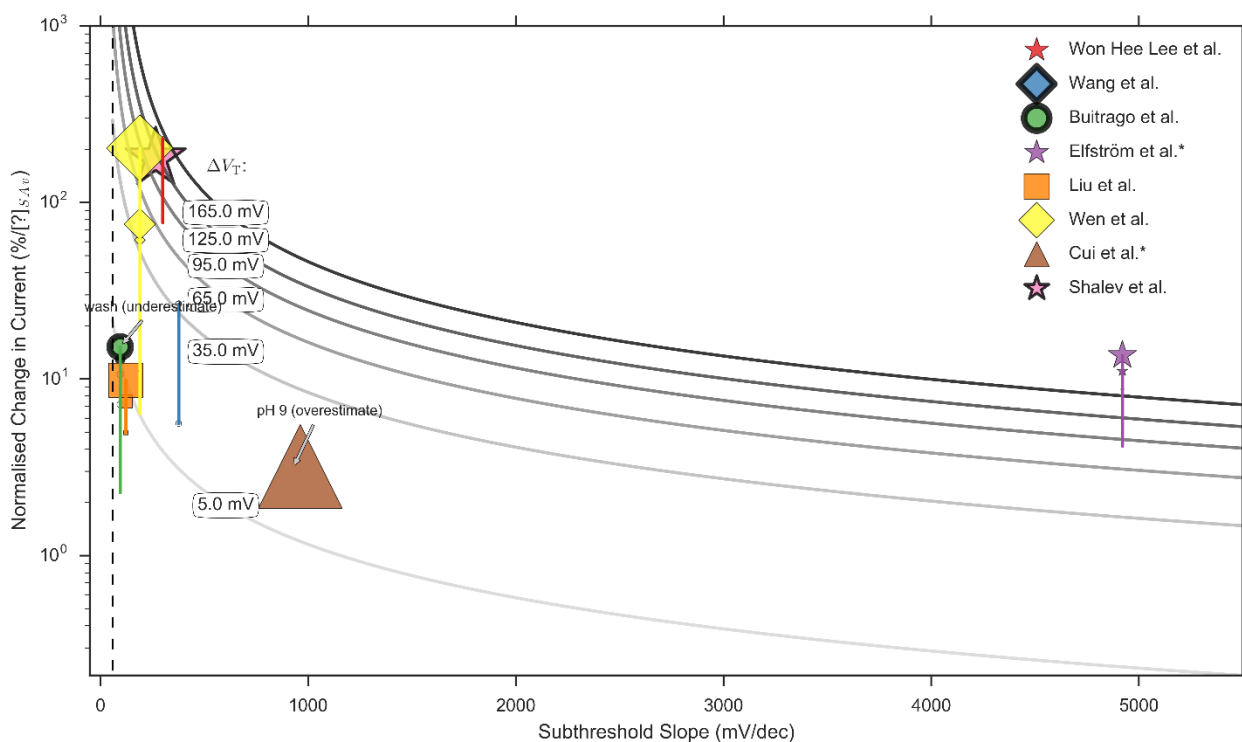


Figure 4 Same plot as Figure 7 from the main text is replotted using a linear x-axis. Measured Normalised Change in Current for streptavidin-sensing data at various concentrations, as a function of Subthreshold Slope.

Linear x-scale

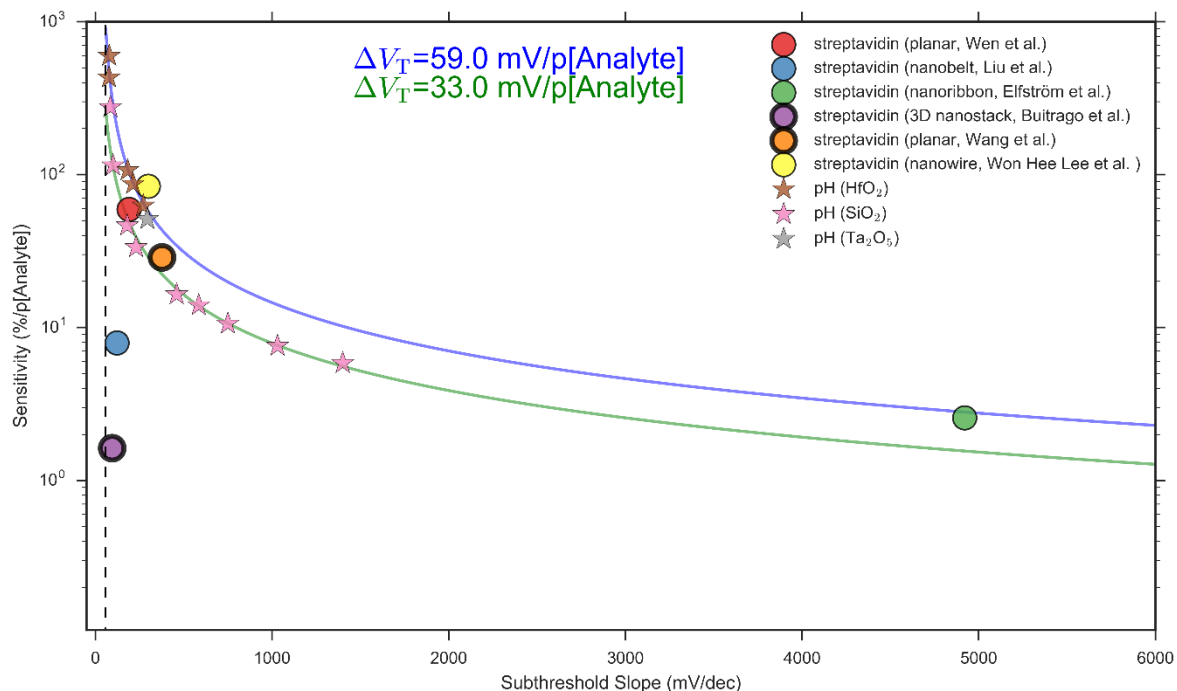


Figure 5 Same plot as Figure 9a in main text but with a linear x-axis. Measured Concentration-dependent current sensitivity ( $I_{norm}^+$  per 10-fold increase in analyte concentration) versus measured Subthreshold Slope, comparing streptavidin sensing (circles) and pH sensing results (stars).

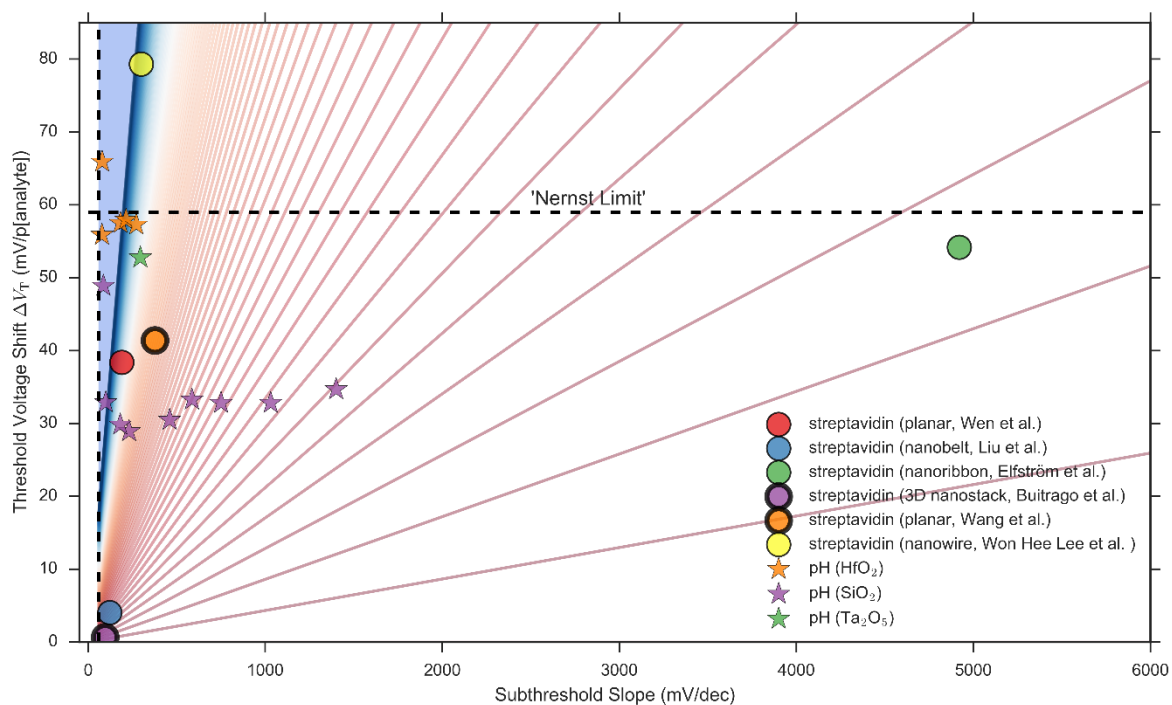


Figure 6: Same plot as Figure 9b in main text but with a linear x-axis. Calculated concentration-dependent surface potential shift versus measured Subthreshold Slope, comparing streptavidin sensing and pH sensing results.

Linear y-scale, log x-scale

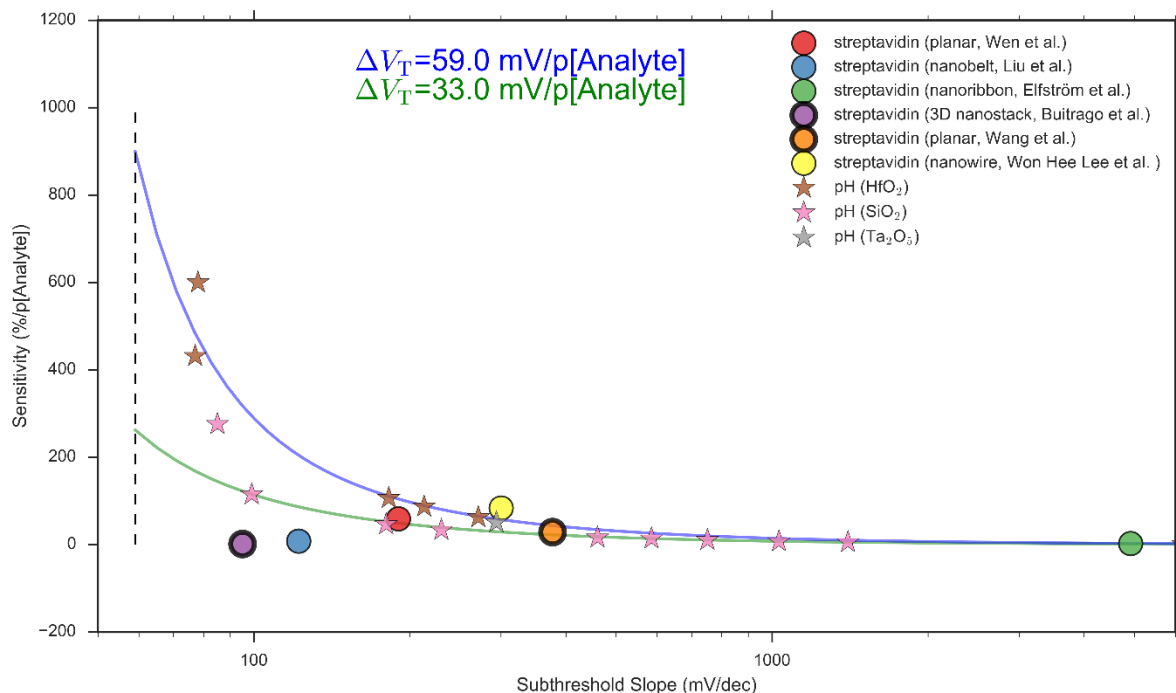


Figure 7: Same plot as Figure 9a in main text but at a linear y-axis scale. Measured Concentration-dependent current sensitivity ( $I_{norm}^+$  per 10-fold increase in analyte concentration) versus measured Subthreshold Slope, comparing streptavidin sensing (circles) and pH sensing results (stars).

Linear y-scale, linear x-scale

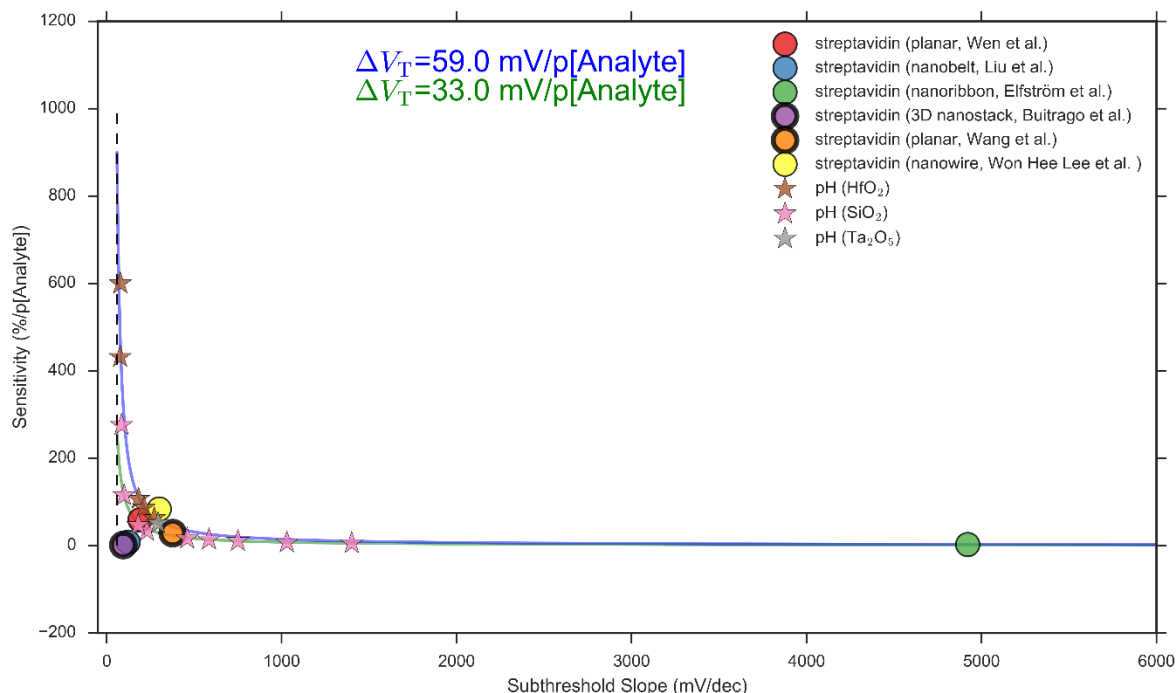


Figure 8: Same plot as Figure 9a in main text but at a linear y-axis scale and linear x-axis scale. Measured Concentration-dependent current sensitivity ( $I_{norm}^+$  per 10-fold increase in analyte concentration) versus measured Subthreshold Slope, comparing streptavidin sensing (circles) and pH sensing results (stars).

## 8 Current-Threshold Voltage Relationships

In this section, the relationship between the change in threshold voltage (e.g. due to analyte binding or a change in gate voltage) and the consequent change in drain-source current through the device. The expressions are based on the drift-diffusion equations.

The transconductance is defined as:

$$g_m = \left. \frac{\delta I_d}{\delta V_g} \right|_{V_{ds}}$$

### Linear Region:

In the linear region, the drain current in the linear region can be described as follows:<sup>11,59</sup>

$$I = \mu_{\text{eff}} C_{\text{ox}} \frac{W}{L} (V_{gs} - V_T) V_{ds} = k_{\text{lin}} (V_g - V_T) V_{ds},$$

where  $k_{\text{lin}}$  is an aggregation of the terms which are constant with respect to a change in gate voltage for a given device (width, length etc.). Assuming that operation is occurring entirely in the linear region then there is no change in transconductance with gate voltage. The transconductance can be obtained from partial differentiation with respect to  $V_g$  at constant  $V_{ds}$ :

$$g_{m,\text{lin}} = k_{\text{lin}} V_{ds}$$

$$\frac{I}{g_{m,\text{lin}}} = \frac{k_{\text{lin}} (V_g - V_T) V_{ds}}{k V_{ds}} = V_g - V_T$$

Assuming  $g_m$  is a constant between  $I_0$  and  $I_f$ :

$$\frac{I_f}{g_{m,\text{lin}}} - \frac{I_0}{g_{m,\text{lin}}} = \frac{\Delta I}{g_{m,\text{lin}}} = [V_g - (V_T - \Delta V_T)] - [V_g - V_T] = \Delta V_T$$

Resulting in the following expression in the linear region:

$$\Delta V_T = \frac{\Delta I}{g_m} \text{ (linear region)}$$

Also it can be noted that the Normalised Change in Current,  $I_{\text{norm}}$ , is a function of the gate voltage in the linear region:

$$I_{\text{norm}} = \frac{I_f - I_0}{I_0} = \frac{\Delta I}{I_0} = \frac{k g_m [V_g - (V_{T,0} - \Delta V_T)] V_{ds} - k g_m [V_g - V_{T,0}] V_{ds}}{k g_m [V_g - V_{T,0}] V_{ds}} = \frac{\Delta V_T}{(V_g - V_{T,0})}$$

This expression has previously been presented by Rajan et al. in order to explain how  $I_{\text{norm}}$  is maximal near the threshold voltage, but that at this point the drain current is low and noise can become a significant component of the response, therefore signal-to-noise is an important figure-of-merit<sup>7</sup>.

$$I_{\text{norm}} = \frac{\Delta V_T}{(V_g - V_{T,0})} \text{ (linear region)}$$

### Subthreshold Region:

In the subthreshold region, the drain current can be described by the following expression<sup>11</sup>:

$$I = k_{\text{sub}} e^{\frac{\ln(10)(V_g - V_T)}{SS}}$$

Where  $k_{\text{sub}}$  is a constant collecting terms which are constant with respect to a change in gate voltage. From partial differentiation at constant  $V_{\text{ds}}$  an expression for the transconductance can be obtained:

Equation 19: 
$$g_{m,\text{sub}} = \frac{k_{\text{sub}} \ln(10)}{SS} e^{\frac{\ln(10)(V_{\text{g}} - V_{\text{T}})}{SS}} = \frac{\ln(10)}{SS} I$$

$g_{\text{m}}$  is a function of  $V_{\text{T}}$  which changes with analyte binding, so at  $I_{\text{f}}$  and  $I_{\text{o}}$   $g_{\text{m}}$  is not constant. It can be seen that  $g_{\text{m}}$  is not a constant in the subthreshold regime after analyte binding, as it is dependent upon  $V_{\text{g}} - V_{\text{T}}$ , and there is a shift in the threshold voltage upon binding of the analyte.  $g_{\text{m}}$  cannot be treated as a constant like in the previous (linear region) derivation, and therefore in order to provide a simple expression relating the shift in threshold voltage and current response, a different approach is required.

It is also possible to express the Normalised Change in Current in terms of the threshold voltage:

$$I_{\text{norm}} = \frac{I_{\text{f}} - I_{\text{i}}}{I_{\text{i}}} = \frac{\Delta I}{I_{\text{i}}} = \frac{ke^{\frac{\ln(10)(V_{\text{g}} - (V_{\text{T}} - \Delta V_{\text{T}}))}{SS}} - ke^{\frac{\ln(10)(V_{\text{g}} - V_{\text{T}})}{SS}}}{ke^{\frac{\ln(10)(V_{\text{g}} - V_{\text{T}})}{SS}}} = e^{\frac{\ln(10)\Delta V_{\text{T}}}{SS}} - 1$$

Or

$$\frac{SS}{\ln(10)} \ln(I_{\text{norm}} + 1) = \Delta V_{\text{T}}$$

555

Which is equivalent to the simpler expression:

$$SS \log_{10}(I_{\text{norm}} + 1) = \Delta V_{\text{T}} \text{ (subthreshold region)}$$

In this work all devices were treated similarly, regardless of their device type (n- or p- channel) such that their  $I_{\text{norm}}$  sensitivities can be compared, the Subthreshold Slope of all devices was taken to be positive. The unbounded signal,  $I_{\text{norm}}^+$  was then calculated similarly to the pH results of our previous work<sup>121</sup>. In this convention, for p-channel devices the unbounded response would correspond to the increase in current due to addition of (negatively charged) streptavidin, and for n-channel devices this can be interpreted as the increase in current on hypothetical "removal" of streptavidin (reverse time on  $I_{\text{ds}}$ -time plot):

$$I_{\text{norm}}^+ (\text{n - channel device, Streptavidin sensing}) = \frac{I_{\text{high}}}{I_{\text{low}}} - 1 = \frac{I_{\text{o}}}{I_{\text{streptavidin}}} - 1$$

## 9 Linear Region Data

Table 4 summarises the sensitivities, transconductances and threshold voltage shifts for streptavidin-sensing experiments performed in the linear region of FET operation with oxide-APTES-biotin surface chemistry. As discussed in the main text of the review, when the back-gate is used for readout, the measured shift in threshold voltage is amplified and is not directly equivalent to the change in surface potential at electrolyte-oxide interface, therefore shifts measured using the back-gate are indicated as such (with  $\Delta V_{T,back}$ ).

Table 4 Linear Sensing Data. The unbounded Normalised Change in Current,  $I_{norm}$ , is shown, and  $\Delta V_T$  where obtained from the paper itself (usually IV curve extraction) is marked as 'expt.'. Where calculated using  $\Delta V_T = \Delta I / g_m$  it is marked as 'calc.'. Cheng et al. showed a weak response that was within the noise levels of the device (0.1-2%  $I_{norm}^+$  estimated). Buffer concentration shown as the dilution factor of PBS or the approximately equivalent ionic strength if PBS was not used. Sarkar et al. reports an  $I_{norm}$  of ~10% in the linear region at unknown concentration and likely at pH 3. Shown in brackets in the table is data from their I- $V_g$  graph indicating sensitivities up to ~500 % in 0.01X PBS at 10  $\mu$ M of streptavidin  $\ddagger$  Negligible response at pH 7.2, but increased at different pH. \*\* ~100% is observed at  $\sim V_g = -2.5$  V (edge of linear region). \*\*\* Operated with backgate amplification such that the backgate voltage is swept with a fixed top gate voltage, therefore  $\Delta V_T$  does not correspond directly to the surface potential change at the liquid-oxide surface ( $\Delta \psi_s$ ).

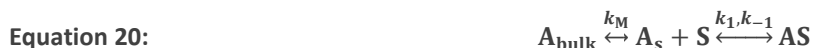
Author	Conc. (nM)	Buffer Conc.	$V_g/V_{T,0}$ (V)	$I_{norm}$ (%)	Sensitivity (%)	$\Delta V_T$ (mV) expt.	$\Delta V_T = \frac{\Delta I}{g_m}$ (mV) calc.
Wen et al. <sup>50</sup>	0.00047 to 4.73	0.25X	0/-3.64	->	0.52	10	NA
Sarkar et al. <sup>53</sup>	0.001 (10,000)	NA (0.01X)	?/? (0.9/?)	10 (500)	-	NA (198)	NA (176.19)
Cheng et al. <sup>58</sup>	0.037	1X	?/-14	0.10 to 2.04 $\ddagger$	-	NA	0.48 to 9.56
Duan et al. <sup>18</sup>	2	0.01X	-2.4/2.22	~ up to 100%**	-	$\Delta V_{T,back} \approx 320$ ***	NA
Nam et al. <sup>80</sup> (WSe <sub>2</sub> device)	0.000001 to	?	-75/~66	->	63	$\Delta V_{T,back} \approx 5000$ ***	NA
Hsiao et al. <sup>75</sup>	0.000167 to 167	0.1X	7/1	->	72	$\Delta V_{T,back} \approx 250$ ***	NA

The top-gate threshold voltage shifts for devices were in the range 0.5 to 44 mV<sup>50,58,59</sup>. Sarkar et al. showed a significantly higher shift (198 mV) which is likely due to the high concentrations of biomolecule (10,000 nM) resulting in non-specific binding.

# 10 Biomolecule Binding Reactions and Kinetics

A detailed discussion of the kinetics of surface-binding can be found within the review by Schuck and Zhao<sup>122</sup> or Squires et al.<sup>123</sup>. Herein important types of systems are outlined – reaction-limited and transport-limited systems, and illustrated via the simple two-compartment model of binding. This model assumes a perfectly flat homogenous plane with equivalent sites in which the analyte binds into an immobile state and is monovalent and homogenous, and all binding events are independent (e.g. no interactions between adsorbate molecules).

In this model, the system is modelled as shown in Equation 20 in which a surface is functionalised with a receptor (S). Addition of an analyte to the bulk ( $A_{\text{bulk}}$ ) will first involve mass transport to a region close to the surface. Molecules within this region ( $A_s$ ) can either form a surface-bound complex or transport back into the bulk:



## 10.1 Reaction-Limited Systems

In reaction-limited systems, whereby the reaction-rate is slower than the rate of mass transport to the surface (i.e.  $K_d$  is high), the replenishment of analyte from the bulk is always faster than its consumption at the sensor surface i.e.  $[A_{\text{bulk}}] = [A]_s$ , and therefore Equation 22 can be simplified to the well-known first-order Langmuir isotherm (Equation 24).



The rate equation for which is shown below, whereby  $[S_{\text{max}}] = [S] + [AS]$ :<sup>18</sup>

**Equation 22:**

$$\frac{d[AS]}{dt} = k_1 [A]_s ([S]_{\text{max}} - [AS]) - k_{-1} [AS]$$

Solving the rate equation can be performed analytically and is shown in Equation 23. This predicts that as the system is left to equilibrate, the bound-concentration will increase as a function of time in an exponential manner according to the following equation:

**Equation 23:**

$$[AB]_t = \frac{k_1 [S]_{\text{max}} [A]_s}{k_1 [A]_s + k_{-1}} (1 - e^{-(k_1 [A]_s + k_{-1})t})$$

From this expression, at equilibrium, the Langmuir isotherm is obtained:

**Equation 24:**

$$\frac{[AS]}{[S]_{\text{max}}} = \frac{[A]_s}{[A]_s + K_d}$$

The equilibrium fraction of occupied sites ( $[AS]/[S]_{\text{max}}$ ) represents the extent of biomolecule binding which will induce a change in surface potential. The response is therefore modelled to be proportional to  $([A]_s/[A]_s + K_d)$ , which in the linear regime corresponds directly to a measured  $\Delta V_T$  response and in the subthreshold regime will correspond to an exponential relationship with surface potential as described in the main text of the review.  $[A]_s$  represents the equilibrium concentration of unbound analyte at the surface at equilibrium, this often cannot be measured directly but is often approximated as the initial added concentration of analyte but this must be done with care. A reaction-limited system has been assumed, therefore  $[A_{\text{bulk}}] = [A]_s$ ; however for this to be valid, the concentration of receptors must be much less than the  $K_d$  of the analyte<sup>124</sup> such that the bulk concentration of analyte does not significantly deplete.

## 10.2 Mass Transport-limited Systems

In contrast, some systems are mass transport-/diffusion- limited, in which the rate of diffusion is slower than the reaction-rate at the surface whereby the  $K_d$  is very small. This is the case for streptavidin-biotin binding<sup>18</sup>. In such systems, the surface-bound concentration  $[A]_s$  is not necessarily equal to the bulk concentration  $[A]_{\text{bulk}}$  as the surface concentration is initially rapidly depleting due to chemical reactions at the surface, and solving the corresponding rate equations cannot be performed analytically. In the two-compartment model for mass transport limited systems, the initial response is expected to be linear as opposed to exponential<sup>122,123</sup>. Given that the bound concentration is proportional to BioFET response, Duan et al. observed an initially linear increase in response on streptavidin-binding which is indicative of mass-transport limited response.<sup>18</sup> Under the assumption that there is sufficient sites on the surface to not deplete the analyte, the time-equilibrated concentrations still correspond to the first-order Langmuir isotherm as described in Equation 24.<sup>7</sup>

## 10.3 Concentration-Dependent Response

Regardless of how the system approaches equilibrium (mass-transport or reaction- limited), the time-equilibrated equilibrium fraction of occupied sites can be described by the Langmuir isotherm in Equation 24<sup>123</sup>. Taking streptavidin-biotin binding as example, the case of 0.1 pM streptavidin in the bulk binding to a biotin functionalised surface is now considered. Assuming that the surface concentration is equal to the bulk concentration, in that the analyte is not being depleted significantly from the bulk concentration and the chemical equilibrium has been reached (i.e. time-equilibrated), then 0.1 pM concentration is present at the surface. Given the 0.001 pM  $K_d$  of the streptavidin, the equilibrium fraction of occupied sites from Equation 24 is predicted to be 0.99 (99% occupied), whereas at 0.01 pM, (0.909) 91% occupancy is expected. A concentration-dependent response is expected and at concentrations of  $\sim 100 K_d$ , the sensor surface is expected to be highly saturated with biomolecule. The dynamic range of a sensor can therefore be seen to be bounded on the upper-limit by the  $K_d$  (higher  $K_d$  = higher dynamic range). Also from Equation 24 it can be shown that that the lower-extent of the dynamic range is bounded by the critical concentration at which only one target molecule binds the sensor at equilibrium  $c^*$ , to a sensor of area  $A$  with density of receptors  $[S]_{\text{max}}$ <sup>123</sup>:

**Equation 25:**

$$c^* = \frac{K_d}{[S]_{\text{max}}A}$$

Note that it was assumed that the surface concentration is equal to the bulk concentration, which is only likely after time-equilibration such that chemical-equilibrium has been reached, and providing that the number of sites on the surface is not so high as to deplete the bulk reagent concentration. For systems with a high affinity (low  $K_d$ ) like streptavidin-biotin, large concentrations of biomolecule bind to the surface and therefore the surface concentration is depleted and the Langmuir isotherm in Equation 24 is not valid. Rajan (2013) used numerical simulation to highlight how increasing the number of receptors with a low concentration of analyte can result in a reduced equilibrium fractional coverage  $[AS]/[S]_{\text{max}}$ .

# 11 Summary of Nomenclature

---

Summary of symbols used in the main text:

Terminology	Definition
$\Delta\psi_s$	Shift in surface potential (induced by analyte binding)
$\Delta V_T$	Shift in threshold voltage (induced by analyte binding)
$V_g$	Gate voltage (referenced to source contact)
$V_{ds}$	Drain voltage (referenced to source contact)
$SS$	Subthreshold voltage
$q$	Elementary charge
$k_b$	Boltzmann constant
$m$	Body-effect coefficient
$g_m$	Transconductance
$I_{norm}$	Normalised Change in Current
Sensitivity	$I_{norm}$ per 10-fold increase in analyte concentration
$S_I$	Drain current noise power spectral density
top/back (subscript) e.g. $V_{g,top}$	Indicating whether the device is being gated by an electrode in the liquid ('top') or on the substrate ('back')
0 (subscript) e.g. $I_0$	Indicating value prior to introduction of analyte

## 12 References

---

- 1 M. Lambrechts and W. Sansen, in *Biosensors: Microelectrochemical Devices*, CRC Press, 1992, p. 69.
- 2 C. Toumazou and P. Georgiou, *Electron. Lett.*, 2011, **47**, S7–S12.
- 3 E. D. Minot, A. M. Janssens, I. Heller, H. A. Heering, C. Dekker and S. G. Lemay, *Appl. Phys. Lett.*, 2007, **91**, 093507.
- 4 J. Janata, *The Analyst*, 1994, **119**, 2275.
- 5 S. Chen, L. Nyholm, N. Jokilaakso, A. E. Karlström, J. Linnros, U. Smith and S.-L. Zhang, *Electrochem. Solid-State Lett.*, 2011, **14**, J34–J37.
- 6 S. Chen and S.-L. Zhang, *Anal. Chem.*, 2011, **83**, 9546–9551.
- 7 N. K. Rajan, Yale University, 2013.
- 8 F. N. Ishikawa, M. Curreli, C. A. Olson, H.-I. Liao, R. Sun, R. W. Roberts, R. J. Cote, M. E. Thompson and C. Zhou, *ACS Nano*, 2010, **4**, 6914–6922.
- 9 T. Rim, K. Kim, N. Hong, W. Ko, C.-K. Baek, S. Jeon, M. J. Deen, M. Meyyappan, Y.-H. Jeong and J.-S. Lee, *RSC Adv.*, 2013, **3**, 7963–7969.
- 10 M. W. Shinwari, M. J. Deen and D. Landheer, *Microelectron. Reliab.*, 2007, **47**, 2025–2057.
- 11 Y. Taur and T. H. Ning, *Fundamentals of Modern VLSI Devices*, Cambridge University Press, Second Edition., 2013.
- 12 L. Bousse, *J. Chem. Phys.*, 1982, **76**, 5128–5133.
- 13 G. A. Bootsma, N. F. De Rooij and A. van Silfhout, *Sens. Actuators*, 1981, **1**, 111–136.
- 14 P. Bergveld, *Sens. Actuators B Chem.*, 2003, **88**, 1–20.
- 15 P. Bergveld, *IEEE Trans. Biomed. Eng.*, 1972, **BME-19**, 342–351.
- 16 H.-J. Jang and W.-J. Cho, *Sci. Rep.*, 2014, **4**, 5284.
- 17 N. K. Rajan, X. Duan and M. A. Reed, *Wiley Interdiscip. Rev. Nanomed. Nanobiotechnol.*, 2013, **5**, 629–645.
- 18 X. Duan, Y. Li, N. K. Rajan, D. A. Routenberg, Y. Modis and M. A. Reed, *Nat. Nanotechnol.*, 2012, **7**, 401–407.
- 19 J. R. Brews, *Solid-State Electron.*, 1978, **21**, 345–355.
- 20 C. E. Argarana, I. D. Kuntz, S. Birken, R. Axel and C. R. Cantor, *Nucleic Acids Res.*, 1986, **14**, 1871–1882.
- 21 N. M. Green, in *Advances in Protein Chemistry*, ed. J. T. E. and F. M. R. C.B. Anfinsen, Academic Press, 1975, vol. 29, pp. 85–133.
- 22 S.-C. Wu, M. Hassan Qureshi and S.-L. Wong, *Protein Expr. Purif.*, 2002, **24**, 348–356.
- 23 D. Wild, *The Immunoassay Handbook*, Gulf Professional Publishing, 2005.
- 24 L. Chalet and F. J. Wolf, *Arch. Biochem. Biophys.*, 1964, **106**, 1–5.
- 25 A. Pähler, W. A. Hendrickson, M. A. Kolks, C. E. Argaraña and C. R. Cantor, *J. Biol. Chem.*, 1987, **262**, 13933–13937.
- 26 Thermo Scientific, *Avidin-Biotin Technical Handbook*, United States.
- 27 M. M. Shindel, A. Mohraz, D. R. Mumm and S.-W. Wang, *Langmuir*, 2009, **25**, 1038–1046.
- 28 N. M. Green, in *Methods in Enzymology*, ed. M. W. and E. A. Bayer, Academic Press, 1990, vol. 184, pp. 51–67.
- 29 S. Sivasankar, S. Subramaniam and D. Leckband, *Proc. Natl. Acad. Sci.*, 1998, **95**, 12961–12966.
- 30 Rockland Inc., *Streptavidin Properties and Characterization*, .
- 31 L. Almonte, E. Lopez-Elvira and A. M. Baró, *ChemPhysChem*, 2014, **15**, 2768–2773.
- 32 A. T. Marttila, O. H. Laitinen, K. J. Airene, T. Kulik, E. A. Bayer, M. Wilchek and M. S. Kulomaa, *FEBS Lett.*, 2000, **467**, 31–36.
- 33 S.-C. Wu and S.-L. Wong, *J. Biol. Chem.*, 2005, **280**, 23225–23231.
- 34 M. Howarth, W. Liu, S. Puthenveetil, Y. Zheng, L. F. Marshall, M. M. Schmidt, K. D. Wittrup, M. G. Bawendi and A. Y. Ting, *Nat. Methods*, 2008, **5**, 397–399.
- 35 L. De Vico, L. Iversen, M. H. Sørensen, M. Brandbyge, J. Nygård, K. L. Martinez and J. H. Jensen, *Nanoscale*, 2011, **3**, 3635.
- 36 T. Windbacher, V. Sverdllov and S. Selberherr, in *Biomedical Engineering Systems and Technologies*, Springer, 2010, pp. 85–95.
- 37 N. Lloret, R. S. Frederiksen, T. C. Møller, N. I. Rieben, S. Upadhyay, L. D. Vico, J. H. Jensen, J. Nygård and K. L. Martinez, *Nanotechnology*, 2013, **24**, 035501.
- 38 S. Hideshima, T. Nakamura, S. Kuroiwa and T. Osaka, *ECS Trans.*, 2011, **35**, 121–124.
- 39 S. Hideshima, H. Einati, T. Nakamura, S. Kuroiwa, Y. Shacham-Diamand and T. Osaka, *J. Electrochem. Soc.*, 2010, **157**, J410.
- 40 *Molecular Operating Environment (MOE) Software*, Chemical Computing Group Inc, 010 Sherbooke St. West, Suite #910, Montreal, QC, Canada, H3A 2R7, 2013.
- 41 H. Li, A. D. Robertson and J. H. Jensen, *Proteins Struct. Funct. Bioinforma.*, 2005, **61**, 704–721.
- 42 D. C. Bas, D. M. Rogers and J. H. Jensen, *Proteins Struct. Funct. Bioinforma.*, 2008, **73**, 765–783.
- 43 S. O. Farrell, F. A. Bettelheim, O. Torres, M. K. Campbell and W. H. Brown, *Introduction to General, Organic and Biochemistry*, Brooks/Cole, Pacific Grove, Calif.; Andover, International ed of 10th Revised ed edition., 2011.

- 44 P. C. Weber, D. H. Ohlendorf, J. J. Wendoloski and F. R. Salemme, *Science*, 1989, **243**, 85–88.
- 45 T. Sano and C. R. Cantor, *J. Biol. Chem.*, 1990, **265**, 3369–3373.
- 46 E. Buitrago, École Polytechnique Fédérale de Lausanne, 2014.
- 47 Y. Cui, Q. Wei, H. Park and C. M. Lieber, *Science*, 2001, **293**, 1289–1292.
- 48 E. Stern, J. F. Klemic, D. A. Routenberg, P. N. Wyrembak, D. B. Turner-Evans, A. D. Hamilton, D. A. LaVan, T. M. Fahmy and M. A. Reed, *Nature*, 2007, **445**, 519–522.
- 49 G. Shalev, A. Cohen, A. Doron, A. Machauf, M. Horesh, U. Virobnik, D. Ullien and I. Levy, *Sensors*, 2009, **9**, 4366–4379.
- 50 X. Wen, S. Gupta, Y. Wang, T. R. N. Iii, S. C. Lee and W. Lu, *Appl. Phys. Lett.*, 2011, **99**, 043701.
- 51 X. Wen, S. Gupta, T. R. Nicholson, S. C. Lee and W. Lu, *Phys. Status Solidi C*, 2011, **8**, 2489–2491.
- 52 X. Wen, M. L. Schuette, S. K. Gupta, T. R. Nicholson, S. C. Lee and W. Lu, *IEEE Sens. J.*, 2011, **11**, 1726–1735.
- 53 D. Sarkar, W. Liu, X. Xie, A. C. Anselmo, S. Mitragotri and K. Banerjee, *ACS Nano*, 2014, **8**, 3992–4003.
- 54 E. Buitrago, M. F.-B. Badia, Y. M. Georgiev, R. Yu, O. Lotty, J. D. Holmes, A. M. Nightingale, H. M. Guerin and A. M. Ionescu, *Sens. Actuators B Chem.*, 2014, **199**, 291–300.
- 55 E. Buitrago, M. Fernández-Bolaños, Y. M. Georgiev, R. Yu, O. Lotty, J. D. Holmes, A. M. Nightingale and A. M. Ionescu, in *Proceedings of Technical Program - 2014 International Symposium on VLSI Technology, Systems and Application (VLSI-TSA)*, 2014, pp. 1–2.
- 56 E. Buitrago, M. F. B. Badia, Y. M. Georgiev, R. Yu, O. Lotty, J. D. Holmes, A. M. Nightingale and A. M. Ionescu, in *Device Research Conference (DRC), 2013 71st Annual*, 2013, vol. Supplement, pp. 1–2.
- 57 H. H. Liu, T. H. Lin and J.-T. Sheu, *Sens. Actuators B Chem.*, 2014, **192**, 111–116.
- 58 Y. Cheng, K.-S. Chen, N. L. Meyer, J. Yuan, L. S. Hirst, P. B. Chase and P. Xiong, *Biosens. Bioelectron.*, 2011, **26**, 4538–4544.
- 59 F. N. Ishikawa, M. Curreli, H.-K. Chang, P.-C. Chen, R. Zhang, R. J. Cote, M. E. Thompson and C. Zhou, *ACS Nano*, 2009, **3**, 3969–3976.
- 60 F. Ishikawa, University of Southern California, 2009.
- 61 N. Elfström, A. E. Karlström and J. Linnros, *Nano Lett.*, 2008, **8**, 945–949.
- 62 N. Elfström and J. Linnros, *Nanotechnology*, 2008, **19**, 235201.
- 63 N. Elfström, Royal Institute of Technology, 2008.
- 64 J. Linnros, 2016.
- 65 H. H. Lee, M. Bae, S.-H. Jo, J.-K. Shin, D. H. Son, C.-H. Won and J.-H. Lee, *Sens. Mater.*, , DOI:10.18494/SAM.2015.1092.
- 66 M. T. Martínez, Y.-C. Tseng, M. González and J. Bokor, *J. Phys. Chem. C*, 2012, **116**, 22579–22586.
- 67 X. Duan, L. Mu, S. D. Sawtelle, N. K. Rajan, Z. Han, Y. Wang, H. Qu and M. A. Reed, *Adv. Funct. Mater.*, 2015, **25**, 2279–2286.
- 68 S. Upadhyay, R. Frederiksen, N. Lloret, L. De Vico, P. Krogstrup, J. H. Jensen, K. L. Martinez and J. Nygård, *Appl. Phys. Lett.*, 2014, **104**, 203504.
- 69 S. Gupta, M. Elias, X. Wen, J. Shapiro, L. Brillson, W. Lu and S. C. Lee, *Biosens. Bioelectron.*, 2008, **24**, 505–511.
- 70 A. Star, J.-C. P. Gabriel, K. Bradley and G. Grüner, *Nano Lett.*, 2003, **3**, 459–463.
- 71 K. Bradley, M. Briman, A. Star and G. Grüner, *Nano Lett.*, 2004, **4**, 253–256.
- 72 B. S. Kang, F. Ren, L. Wang, C. Lofton, W. W. Tan, S. J. Pearton, A. Dabiran, A. Osinsky and P. P. Chow, *Appl. Phys. Lett.*, 2005, **87**, 023508.
- 73 A. Choi, K. Kim, H.-I. Jung and S. Y. Lee, *Sens. Actuators B Chem.*, 2010, **148**, 577–582.
- 74 P. Ginet, S. Akiyama, N. Takama, H. Fujita and B. Kim, *J. Micromechanics Microengineering*, 2011, **21**, 065008.
- 75 C.-Y. Hsiao, C.-H. Lin, C.-H. Hung, C.-J. Su, Y.-R. Lo, C.-C. Lee, H.-C. Lin, F.-H. Ko, T.-Y. Huang and Y.-S. Yang, *Biosens. Bioelectron.*, 2009, **24**, 1223–1229.
- 76 K. A. Jeon, H. J. Son, C. E. Kim, M. S. Shon, K. H. Yoo, A. M. Choi, H. I. Jung and Sang, *IEEE*, 2006, pp. 1265–1268.
- 77 D. Khatayevich, T. Page, C. Gresswell, Y. Hayamizu, W. Grady and M. Sarikaya, *Small*, 2014, **10**, 1505–1513.
- 78 J. S. Kim, W. I. Park, C.-H. Lee and G.-C. Yi, *Korean Phys. Soc.*, 2006, **49**, 1635.
- 79 Won Hee Lee, Jin-Moo Lee, Mihee Uhm, Jieun Lee, Kyung Rok Kim, Sung-Jin Choi, Dong Myong Kim, Yong-Joo Jeong and Dae Hwan Kim, *IEEE Electron Device Lett.*, 2014, **35**, 587–589.
- 80 H. Nam, B.-R. Oh, M. Chen, S. Wi, D. Li, K. Kurabayashi and X. Liang, *J. Vac. Sci. Technol. B Nanotechnol. Microelectron. Mater. Process. Meas. Phenom.*, 2015, **33**, 06FG01.
- 81 P. Hu, J. Zhang, Z. Wen and C. Zhang, *Nanotechnology*, 2011, **22**, 335502.
- 82 Y. Wang, P. C. Sondergaard, A. Theiss, S. C. Lee and W. Lu, *ECS Trans.*, 2014, **61**, 139–146.
- 83 H. Im, X.-J. Huang, B. Gu and Y.-K. Choi, *Nat. Nanotechnol.*, 2007, **2**, 430–434.
- 84 D.-S. Kim, J.-E. Park, J.-K. Shin, P. K. Kim, G. Lim and S. Shoji, *Sens. Actuators B Chem.*, 2006, **117**, 488–494.
- 85 D.-I. Han, D.-S. Kim, J.-E. Park, J.-K. Shin, S.-H. Kong, P. Choi, J.-H. Lee and G. Lim, *Jpn. J. Appl. Phys.*, 2005, **44**, 5496–5499.
- 86 B. C. Jacquot, N. Muñoz, D. W. Branch and E. C. Kan, *Biosens. Bioelectron.*, 2008, **23**, 1503–1511.

- 87 P. Hu, A. Fasoli, J. Park, Y. Choi, P. Estrela, S. L. Maeng, W. I. Milne and A. C. Ferrari, *J. Appl. Phys.*, 2008, **104**, 074310.
- 88 A. M. Münzer, W. Seo, G. J. Morgan, Z. P. Michael, Y. Zhao, K. Melzer, G. Scarpa and A. Star, *J. Phys. Chem. C*, 2014, **118**, 17193–17199.
- 89 G. S. Kulkarni, W. Zang and Z. Zhong, *Acc. Chem. Res.*, 2016, **49**, 2578–2586.
- 90 G. S. Kulkarni and Z. Zhong, *Nano Lett.*, 2012, **12**, 719–723.
- 91 J. Go, P. R. Nair and M. A. Alam, *J. Appl. Phys.*, 2012, **112**, 034516.
- 92 I. Moore, C. Millar, S. Roy and A. Asenov, in *2010 14th International Workshop on Computational Electronics (IWCE)*, 2010, pp. 1–4.
- 93 I. Moore, C. Millar, S. Roy and A. Asenov, *J. Comput. Electron.*, 2012, **11**, 266–271.
- 94 K. D. Cantley, P. G. Fernandes, M. Zhao, H. J. Stiegler, R. A. Chapman and E. M. Vogel, in *2012 IEEE 55th International Midwest Symposium on Circuits and Systems (MWSCAS)*, 2012, pp. 370–373.
- 95 M. J. Deen, M. W. Shinwari, J. C. Ranuárez and D. Landheer, *J. Appl. Phys.*, 2006, **100**, 074703.
- 96 D. Landheer, G. Aers, W. R. McKinnon, M. J. Deen and J. C. Ranuarez, *J. Appl. Phys.*, 2005, **98**, 044701.
- 97 C. Heitzinger, Y. Liu, N. J. Mauser, C. Ringhofer and R. W. Dutton, *J. Comput. Theor. Nanosci.*, 2010, **7**, 2574–2580.
- 98 F. V. Gasparyan, S. A. Vitusevich, A. Offenhäusser and M. J. Schöning, *Mod. Phys. Lett. B*, 2011, **25**, 831–840.
- 99 N. Clément, K. Nishiguchi, J. F. Dufreche, D. Guerin, A. Fujiwara and D. Vuillaume, *Appl. Phys. Lett.*, 2011, **98**, 014104.
- 100 N. K. Rajan, D. A. Routenberg and M. A. Reed, *Appl. Phys. Lett.*, 2011, **98**, 264107.
- 101 N. K. Rajan, K. Brower, X. Duan and M. A. Reed, *Appl. Phys. Lett.*, 2014, **104**, 084106.
- 102 S. Kim, T. Rim, K. Kim, U. Lee, E. Baek, H. Lee, C.-K. Baek, M. Meyyappan, M. J. Deen and J.-S. Lee, *Analyst*, 2011, **136**, 5012–5016.
- 103 S. Pud, J. Li, V. Sibille, M. Petrychuk, V. Kovalenko, A. Offenhäusser and S. Vitusevich, *Nano Lett.*, 2014, **14**, 578–584.
- 104 S. Romyantsev, G. Liu, M. S. Shur, R. A. Potyraiilo and A. A. Balandin, *Nano Lett.*, 2012, **12**, 2294–2298.
- 105 M.-P. Lu, E. Vire and L. Montès, *Nanotechnology*, 2015, **26**, 495501.
- 106 K. Georgakopoulou, A. Birbas and C. Spathis, *J. Appl. Phys.*, 2015, **117**, 104505.
- 107 G. Zheng, X. P. A. Gao and C. M. Lieber, *Nano Lett.*, 2010, **10**, 3179–3183.
- 108 I. Jokić, M. Frantlović, Z. Djurić, K. Radulović and Z. Jokić, *Microelectron. Eng.*, 2015, **144**, 32–36.
- 109 I. Heller, J. Männik, S. G. Lemay and C. Dekker, *Nano Lett.*, 2009, **9**, 377–382.
- 110 K. Georgakopoulou, A. Birbas and C. Spathis, *J. Appl. Phys.*, 2015, **117**, 104505.
- 111 I.-Y. Chung, J. Lee, M. Seo and C. H. Park, *Jpn. J. Appl. Phys.*, 2016, **55**, 127001.
- 112 H. Ghosh and C. RoyChaudhuri, *Appl. Phys. Lett.*, 2013, **102**, 243701.
- 113 H. Ghosh, D. Kundu and C. RoyChaudhuri, *IEEE Trans. Electron Devices*, 2016, **63**, 3241–3248.
- 114 E. Tombácz, *Chem. Eng.*, 2007, **53**, 77–86.
- 115 N. Sahai, *Environ. Sci. Technol.*, 2002, **36**, 445–452.
- 116 M. A. Brown, Z. Abbas, A. Kleibert, R. G. Green, A. Goel, S. May and T. M. Squires, *Phys. Rev. X*, 2016, **6**, 011007.
- 117 W. M. Siu and R. S. C. Cobbold, *IEEE Trans. Electron Devices*, 1979, **26**, 1805–1815.
- 118 J. L. Diot, J. Joseph, J. R. Martin and P. Clechet, *J. Electroanal. Chem. Interfacial Electrochem.*, 1985, **193**, 75–88.
- 119 L. Bousse, N. F. D. Rooij and P. Bergveld, *IEEE Trans. Electron Devices*, 1983, **30**, 1263–1270.
- 120 C. D. Fung, P. W. Cheung and W. H. Ko, *IRE*, 1980, pp. 689–692.
- 121 K. Sun, I. Zeimpekis, C. Hu, N. M. J. Ditshego, O. Thomas, M. R. R. de Planque, H. M. H. Chong, H. Morgan and P. Ashburn, *Nanotechnology*, 2016, **27**, 285501.
- 122 P. Schuck and H. Zhao, *Methods Mol. Biol. Clifton NJ*, 2010, **627**, 15–54.
- 123 T. M. Squires, R. J. Messinger and S. R. Manalis, *Nat. Biotechnol.*, 2008, **26**, 417–426.
- 124 D. A. Hall and C. J. Langmead, *Br. J. Pharmacol.*, 2010, **161**, 1276–1290.